SUPPLEMENTARY DATA

Vitis vinifera Leaves Extract Liposomal Carbopol Gel Preparation's Potential Wound Healing and Antibacterial Benefits: *In Vivo*, Phytochemical, and Computational Investigation

Abeer H. Elmaidomy[1], Soad A. Mohamad[2], Mahmoud Abdelnaser[3], Ramadan Yahia[4], Fatma A. Mokhtar[5], Faisal Alsenani[6], Motaz Y. Badr[7], Safa Y. Almaghrabi[8], Faisal H. Altemani[9], Mubarak A. Alzubaidi[10], Entesar Ali Saber[11], Mahmoud A. Elrehany[3], Usama Ramadan Abdelmohsen[12,13], Ahmed M. Sayed[14*]

[1]Department of Pharmacognosy, Faculty of Pharmacy, Beni-Suef University, Beni-Suef 62514, Egypt. Abeer011150@pharm.bsu.edu.eg
[2]Department of pharmaceutics and clinical pharmacy, Faculty of Pharmacy, Deraya University, New Minia 61111, Egypt
[3]Department of Biochemistry, Faculty of Pharmacy, Deraya University, New Minia 61111, Egypt
[4]Department of Microbiology and immunology, Faculty of Pharmacy, Deraya University, Universities Zone, New Minia City 1661111, Egypt
[5]Department of Pharmacognosy, Faculty of Pharmacy, ALSalam University, Kafr El Zayat, Egypt
[6]Department of Pharmacognosy, College of Pharmacy, Umm Al-Qura University, Makkah 21955, Saudi Arabia; fssenani@uqu.edu.sa; ORCID: 0000-0002-7267-9636.
[7]Department of Pharmaceutics, College of Pharmacy, Umm Al-Qura University, Makkah 21955, Saudi Arabia; mybadr@uqu.edu.sa; ORCID: 0000-0003-0737-1894.
[8]Department of Physiology, Faculty of Medicine, King Abduaziz University, Jeddah 22252, Saudi Arabia; salmaghrabe@kau.edu.sa ORCID: 0000-0001-5713-6732.
[9]Department of Medical Laboratory Technology, Faculty of Applied Medical Sciences, University of Tabuk, Tabuk 71491, Saudi Arabia.
[10]Department of Biological Sciences, Faculty of Science, King Abdulaziz University, Jeddah 21589, Saudi Arabia.
[11]Department of Histology and Cell Biology, Faculty of Medicine, Minia University, Minia 61519 Egypt, Delegated to Deraya University, Universities Zone, New Minia 61111, Egypt.
[12]Department of Pharmacognosy, Faculty of Pharmacy, Minia University, Minia 61519, Egypt
[13]Department of Pharmacognosy, Faculty of Pharmacy, Deraya University, New Minia 61111.
[14]Department of Pharmacognosy, Faculty of Pharmacy, Nahda University, Beni-Suef 62513, Egypt. 61111, Egypt

Corresponding author: ahmed.mohamed.sayed@nub.edu.eg

Abstract

Vitis vinifera Egyptian edible leaves extract, loaded on Soybean lecithin, cholesterol, and Carbopol gel preparation (VVL-liposomal gel), was prepared to maximize the *in vivo* wound healing, and anti-MRSA activities for the crude extract, using an excision wound model, focusing on TLR-2, MCP-1, CXCL-1, CXCL-2, IL-6 and IL-1β, and MRSA (wound infection model, and peritonitis infection model). VVL-liposomal gel was stable with significant drug entrapment efficiency reached 88%±3; zeta potential value ranging from -50 to -63, and size from 50-200μm nm diameter. The *in vivo* evaluation proved the ability of VVL-liposomal gel to gradually release the drugs in a sustained manner with higher complete wound healing effect and tissue repair after 7 days administration, with significant decrease in bacterial count, comparing with the crude extract. Phytochemical investigation of leaves crude extract yielded fourteen compounds: two new stilbenes (**1, 2)**, with twelve known ones (**3-14)**. Furthermore, a computational study was conducted to identify the genes and possible pathways responsible for the anti-MRSA activity of the isolated compounds. Accompanied with inverse docking to identify the most likely molecular targets that could mediate the extract's antibacterial activity. Gyr-B was discovered to be the best target for compounds 1 and 2. Hence, VVL-liposomal gel can be used as novel anti-dermatophytic agent with potent wound healing, anti-MRSA capacity, which paving the way for future clinical research.

Keywords: *Vitis vinifera*, MRSA, TLR-2, wound healing, docking, Gyr-B.

List of Contents

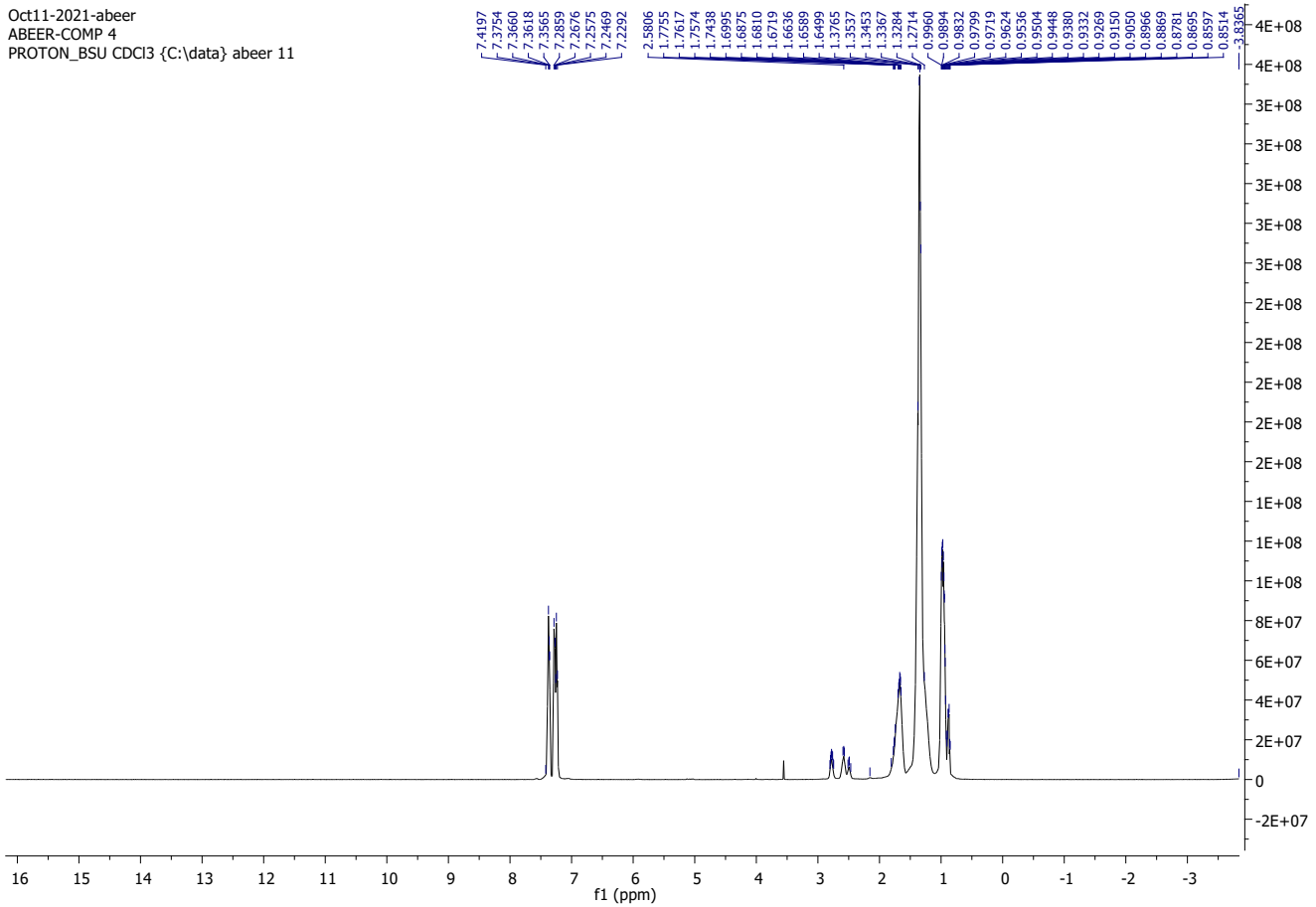

Figure S1. 1H NMR spectrum of compound **1** measured in $CDCL_3$-*d* at 400 MHz

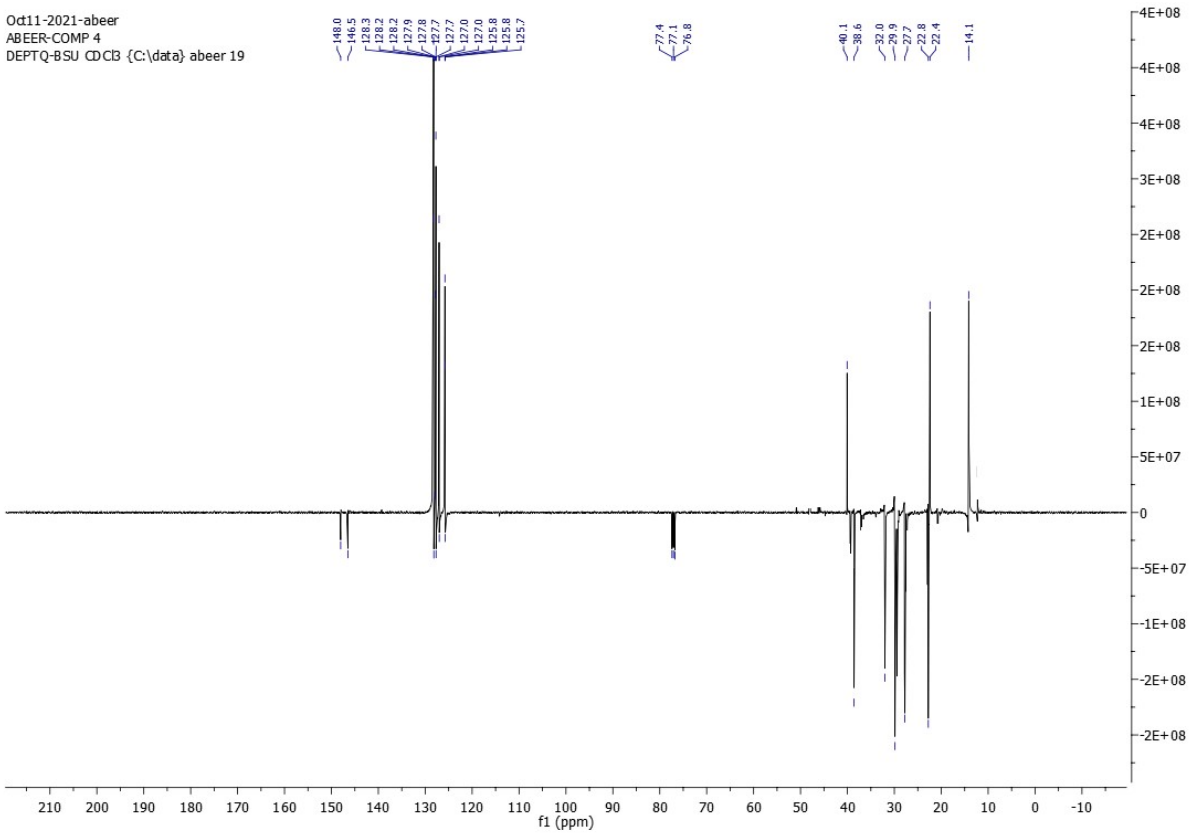

Figure S2. DEPT-Q NMR spectrum of compound **1** measured in $CDCL_3$-*d* at 100 MHz

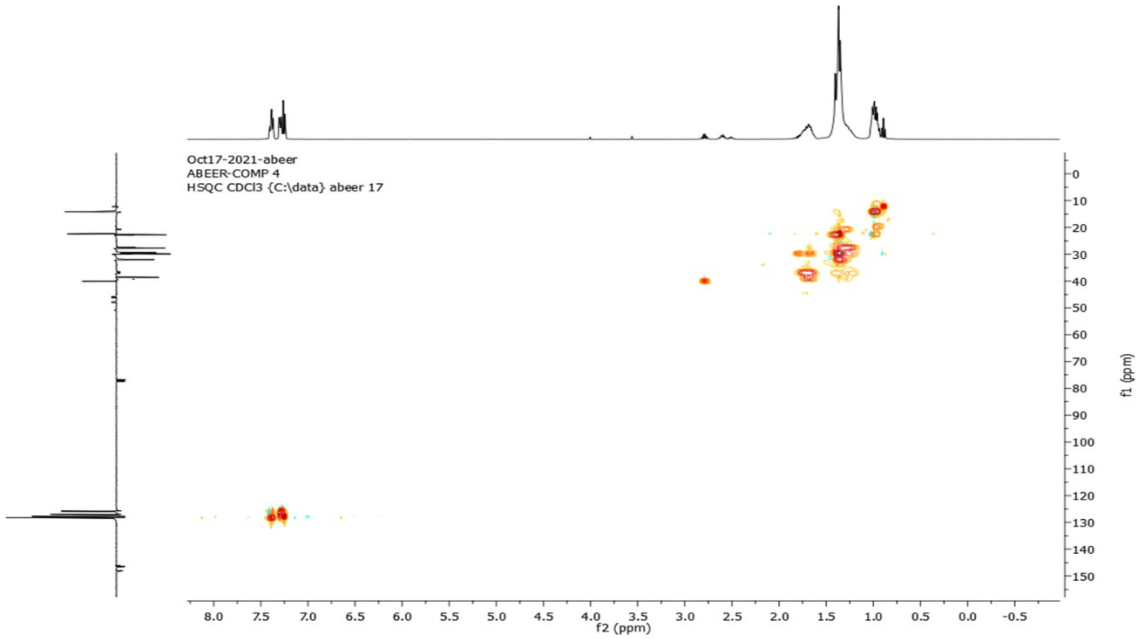

Figure S3. HSQC spectrum of compound **1** measured in $CDCL_3$-*d*

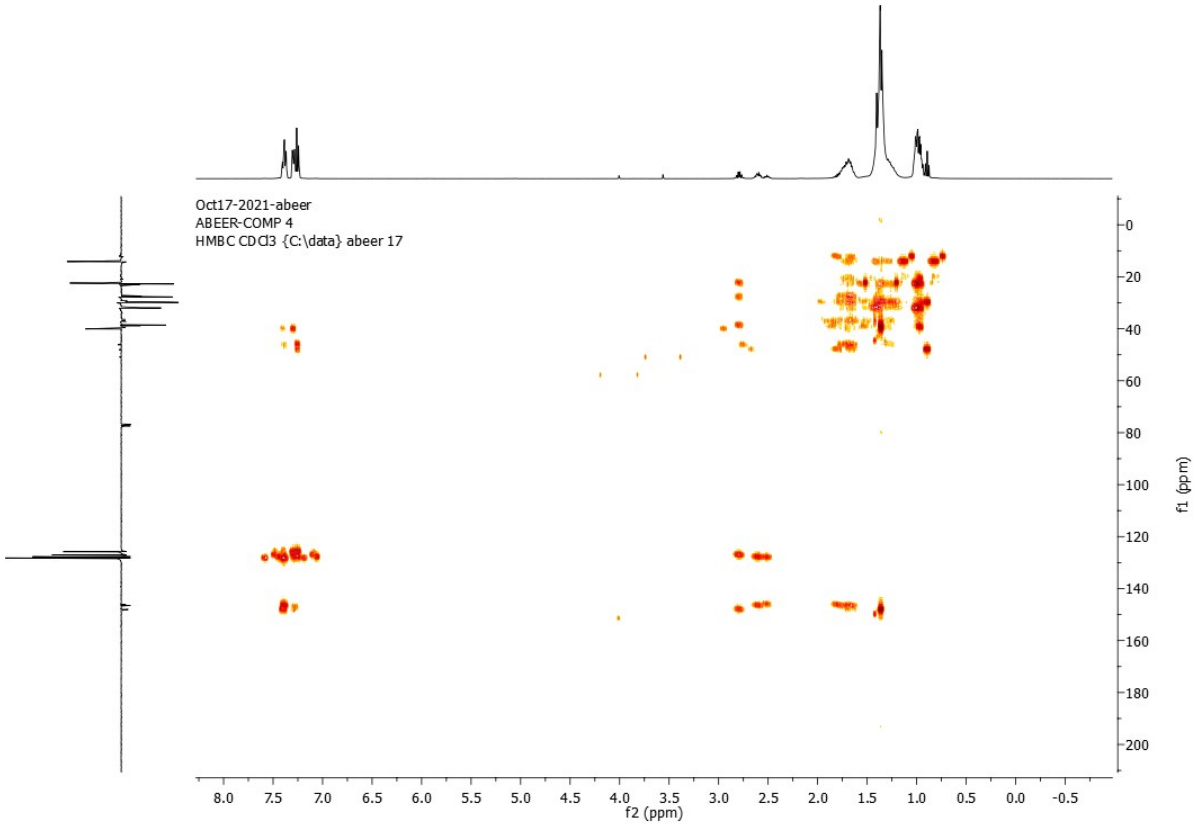

Figure S4. HMBC spectrum of compound **1** measured in $CDCL_3$-*d*

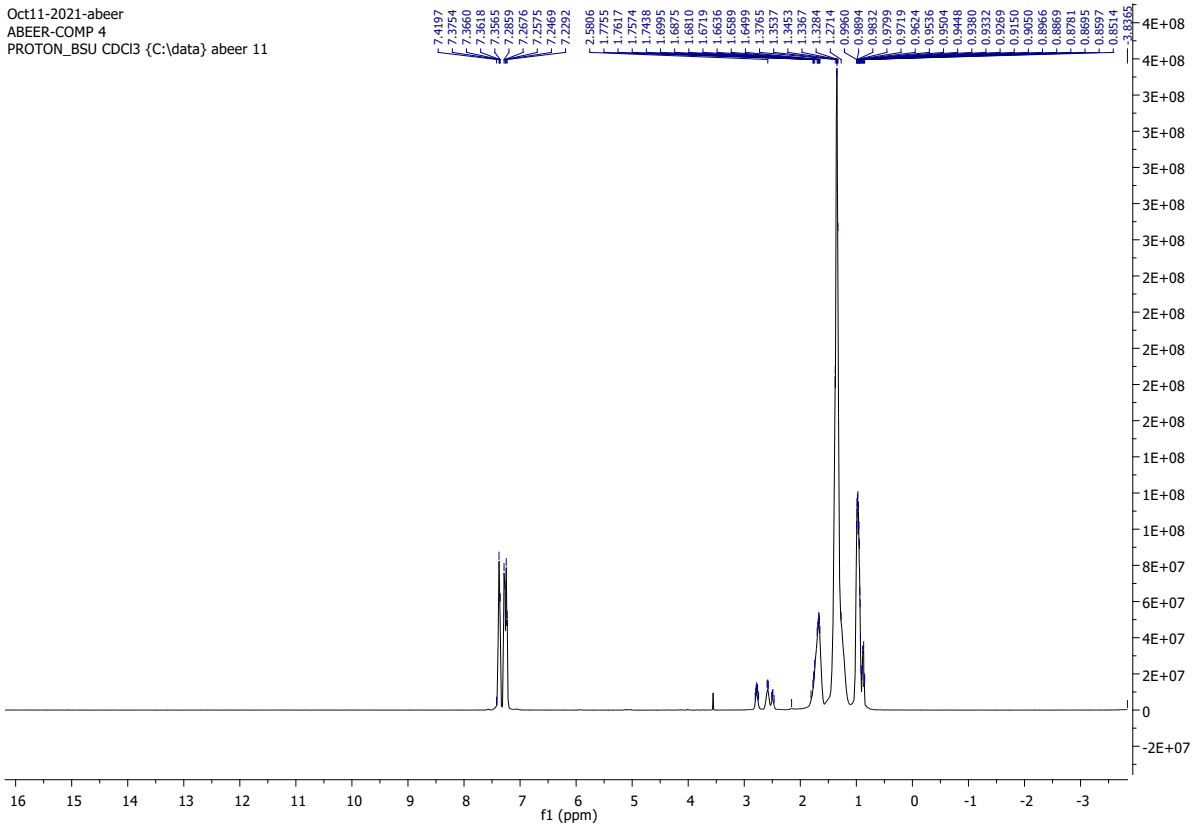

Figure S5. 1H NMR spectrum of compound **2** measured in $CDCL_3$-*d* at 400 MHz

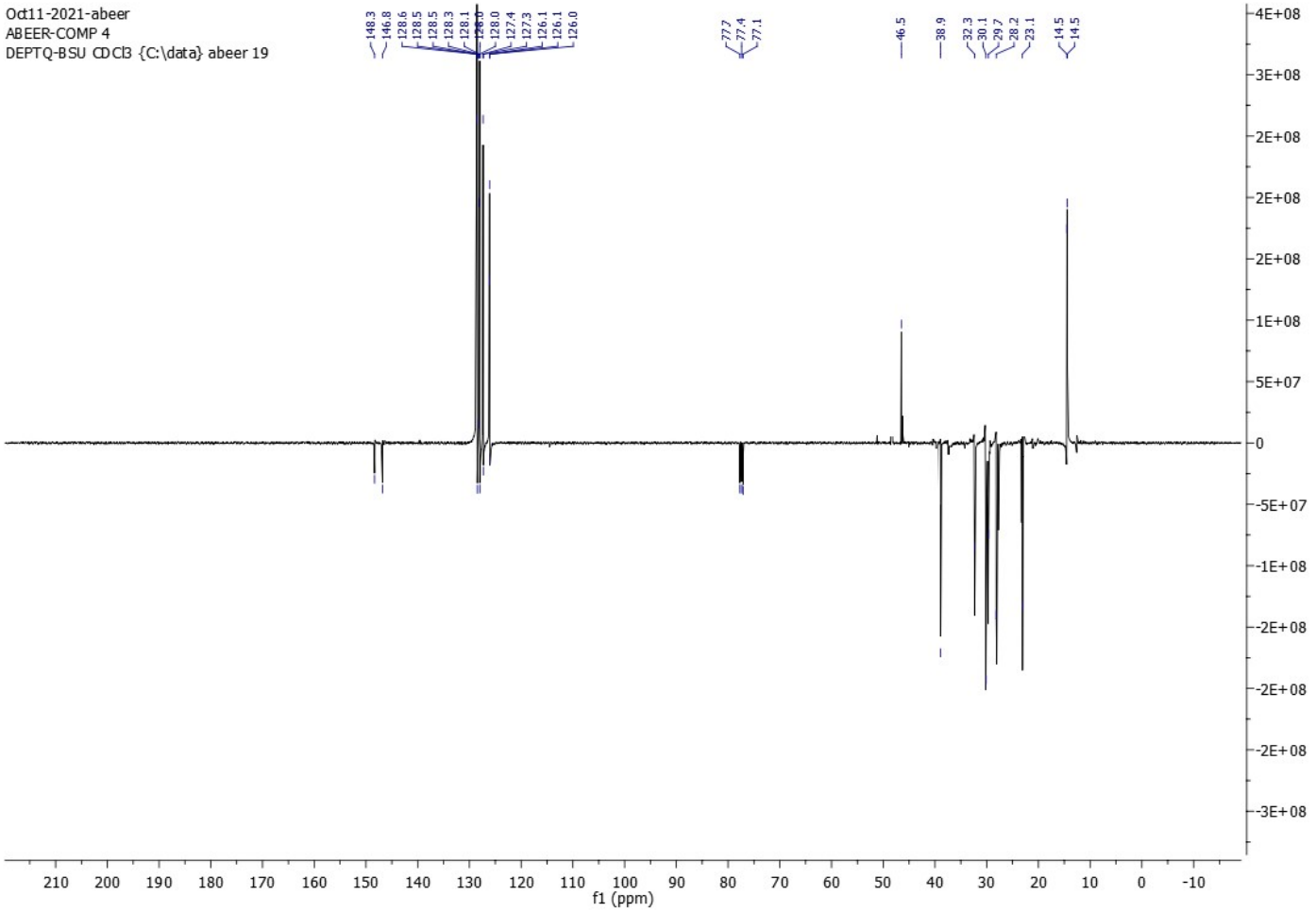

Figure S6. DEPT-Q NMR spectrum of compound **2** measured in $CDCL_3$-*d* at 100 MHz

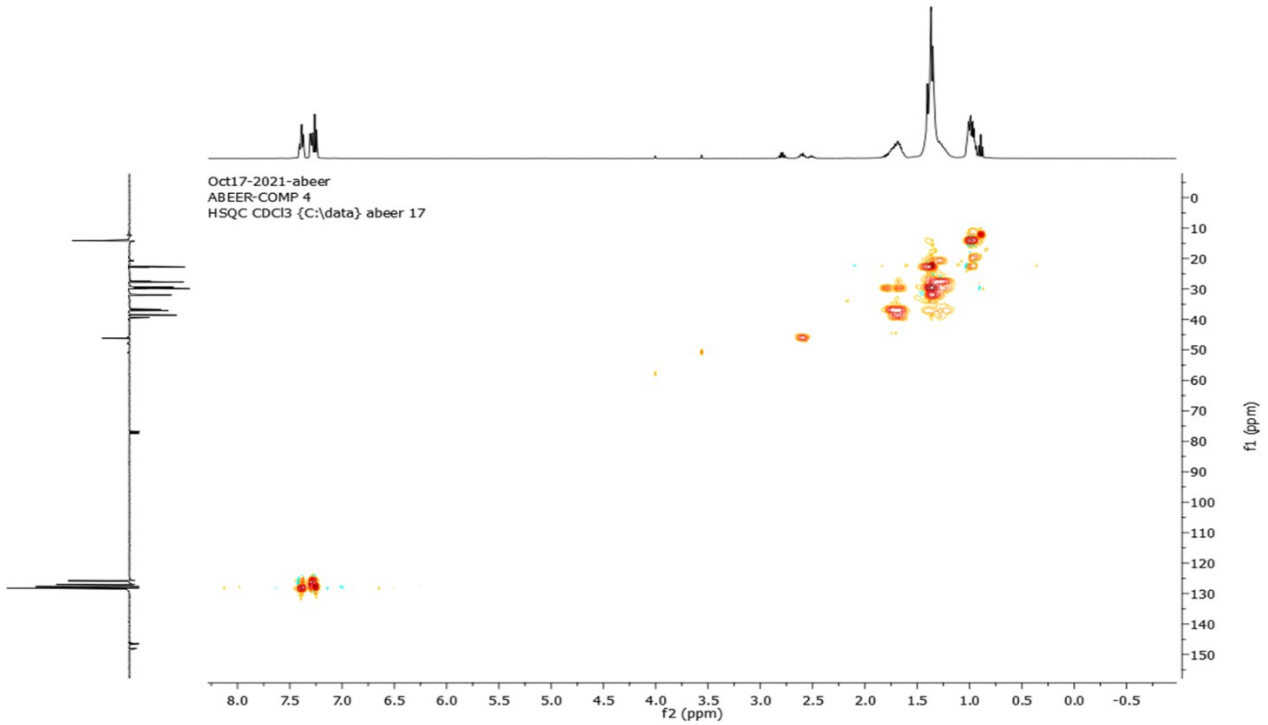

Figure S7. HSQC spectrum of compound **2** measured in $CDCL_3$-*d*

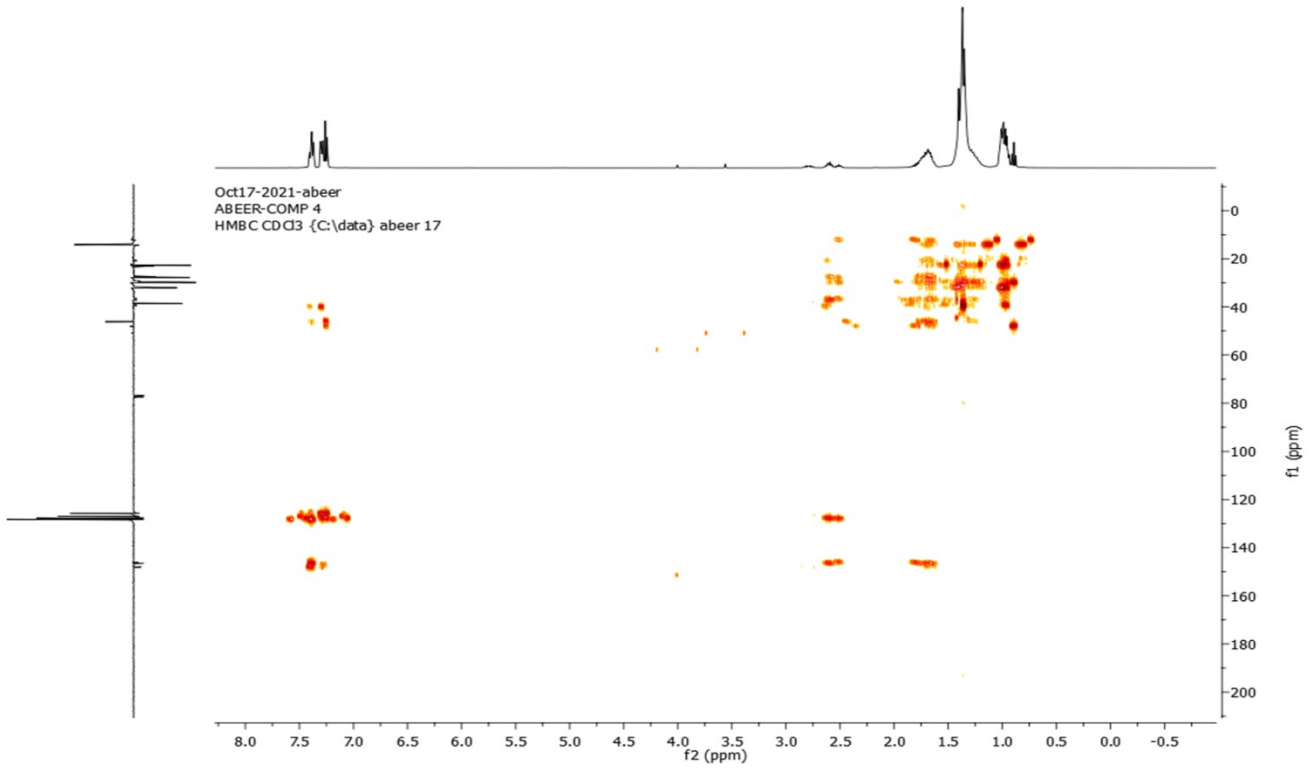

Figure S8. HMBC spectrum of compound **2** measured in $CDCL_3$-*d*

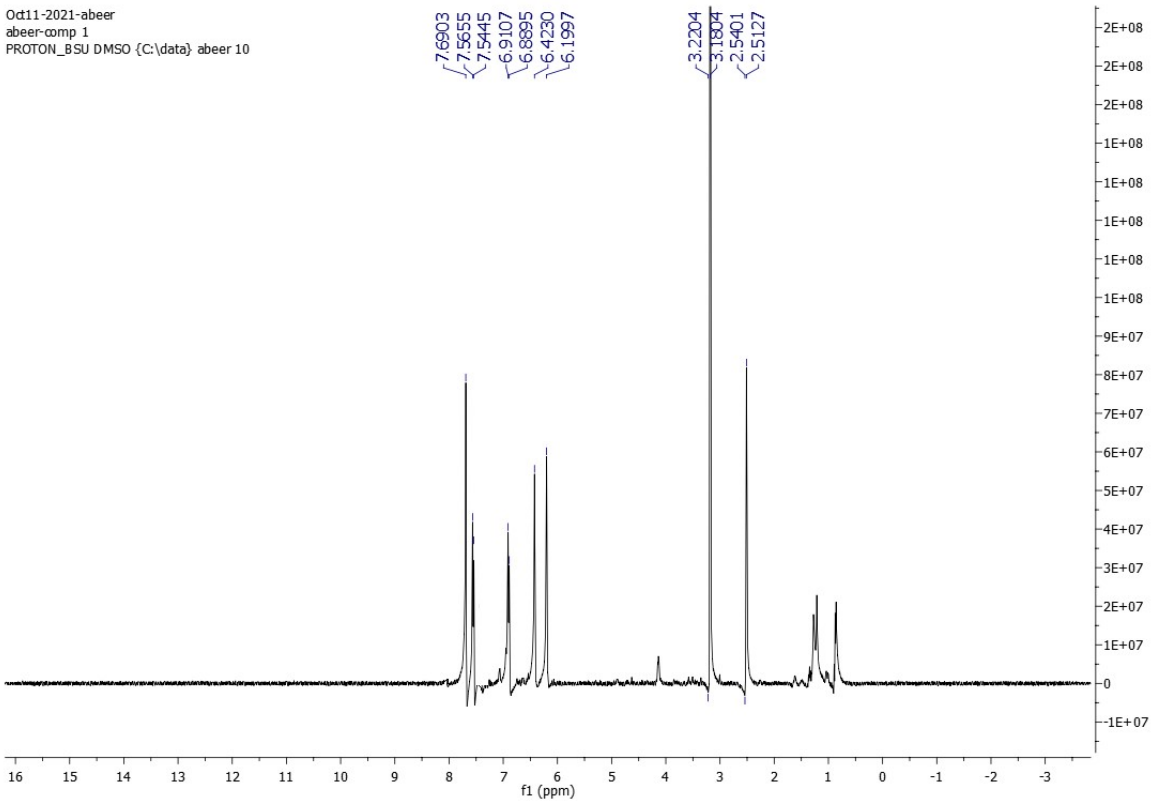

Figure S9. 1H NMR spectrum of compound **3** measured in DMSO-d_6 at 400 MHz

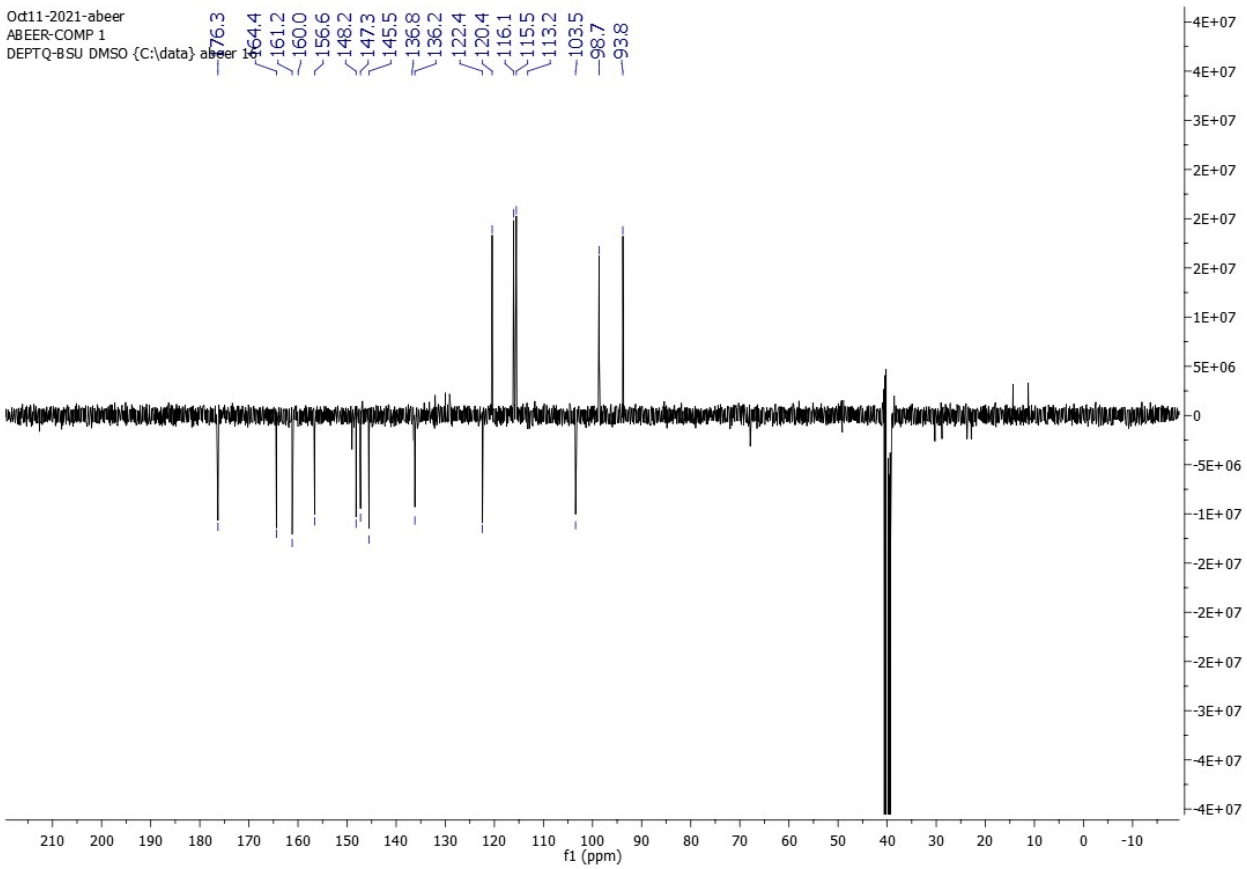

Figure S10. DEPT-Q NMR spectrum of compound **3** measured in DMSO-d_6 at 100 MHz

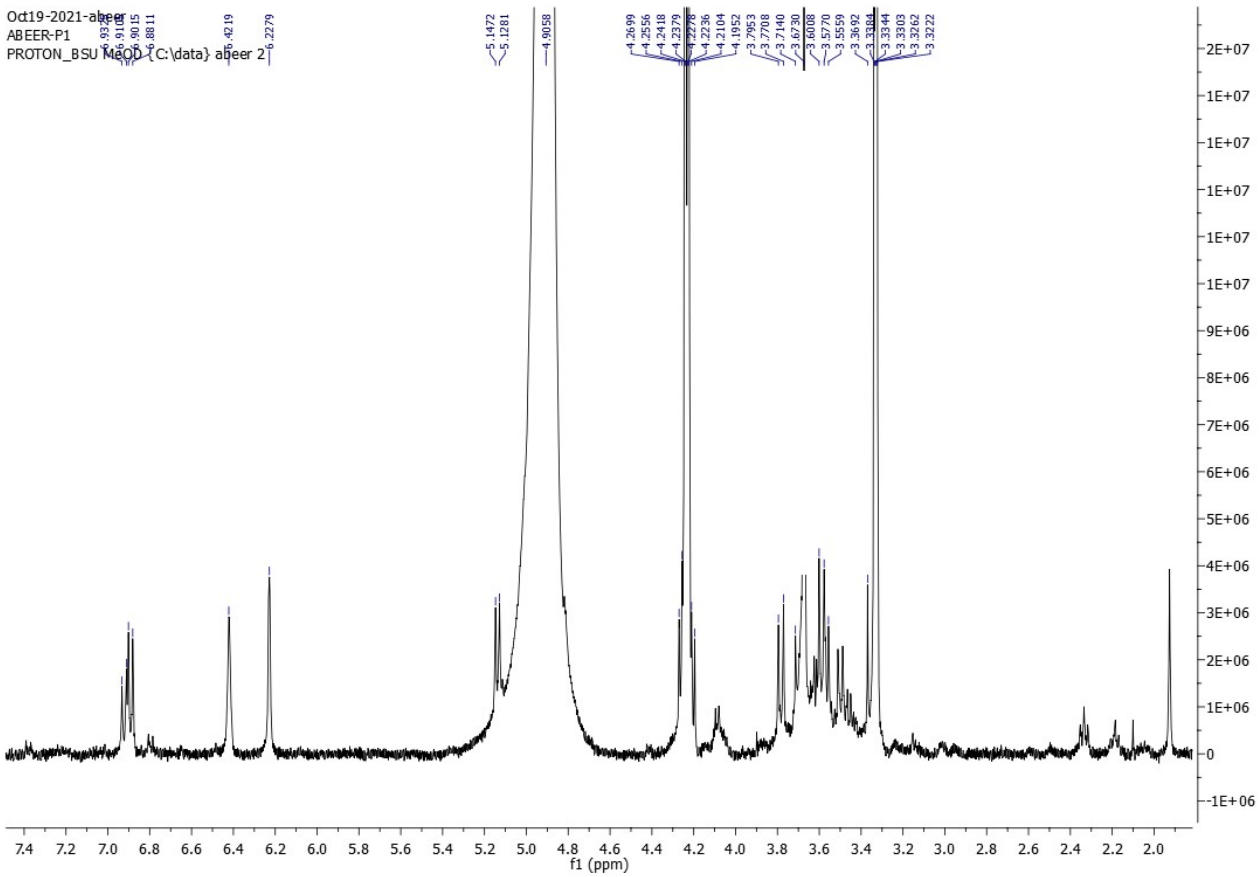

Figure S11. 1H NMR spectrum of compound **4** measured in CD_3OD-d_4 400 MHz

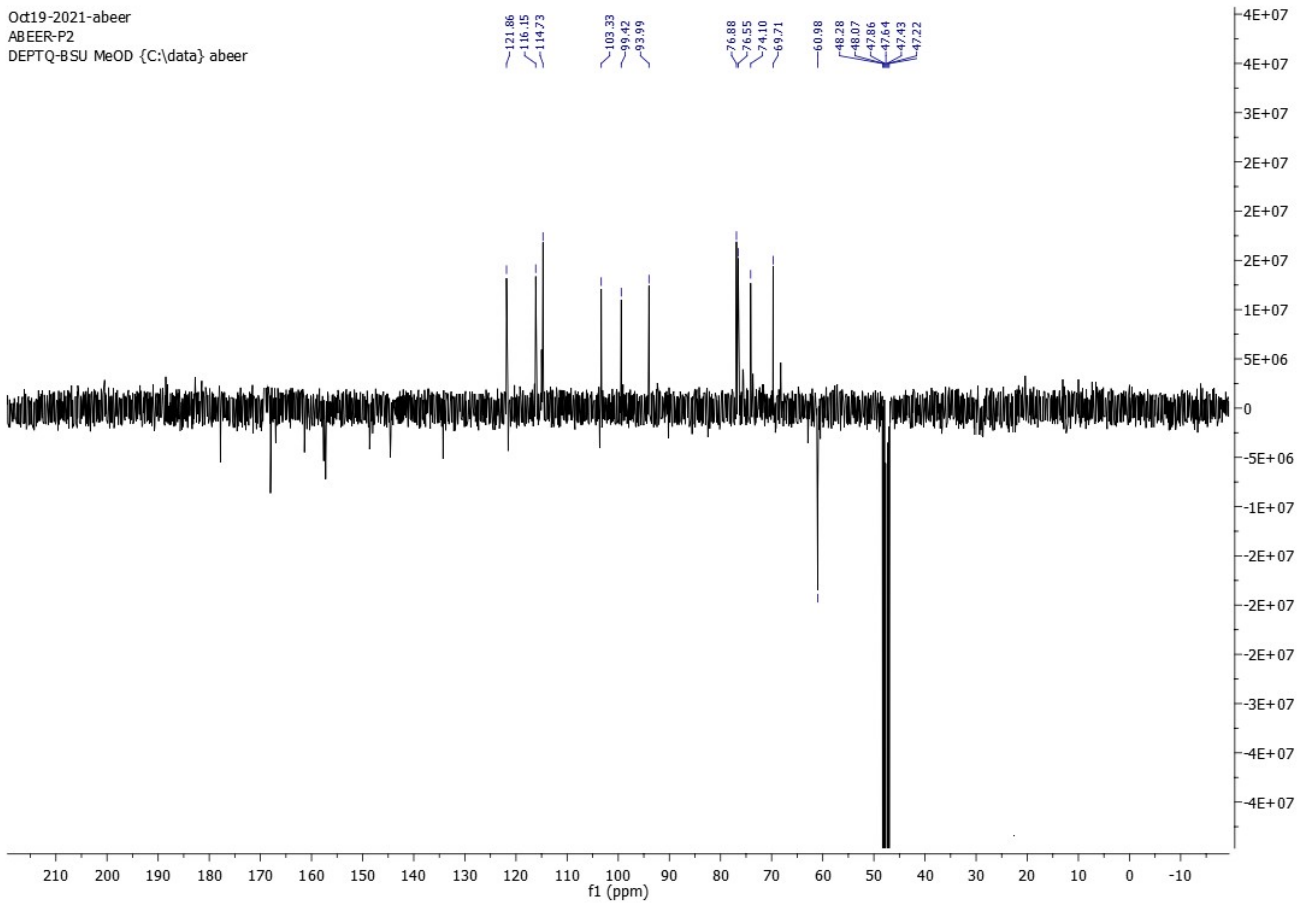

Figure S12. DEPT-Q NMR spectrum of compound **4** measured in CD_3OD-d_4 at 100 MHz

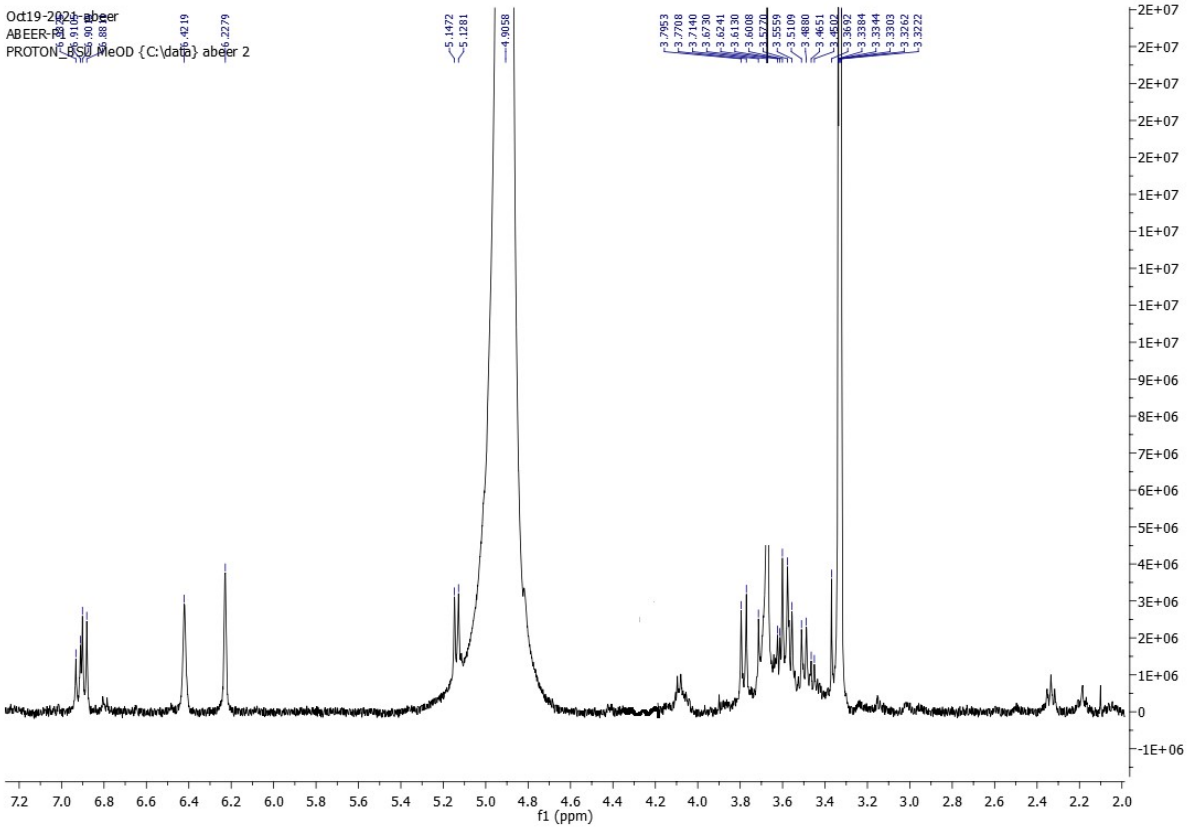

Figure S13. 1H NMR spectrum of compound **5** measured in CD_3OD-d_4 at 400 MHz

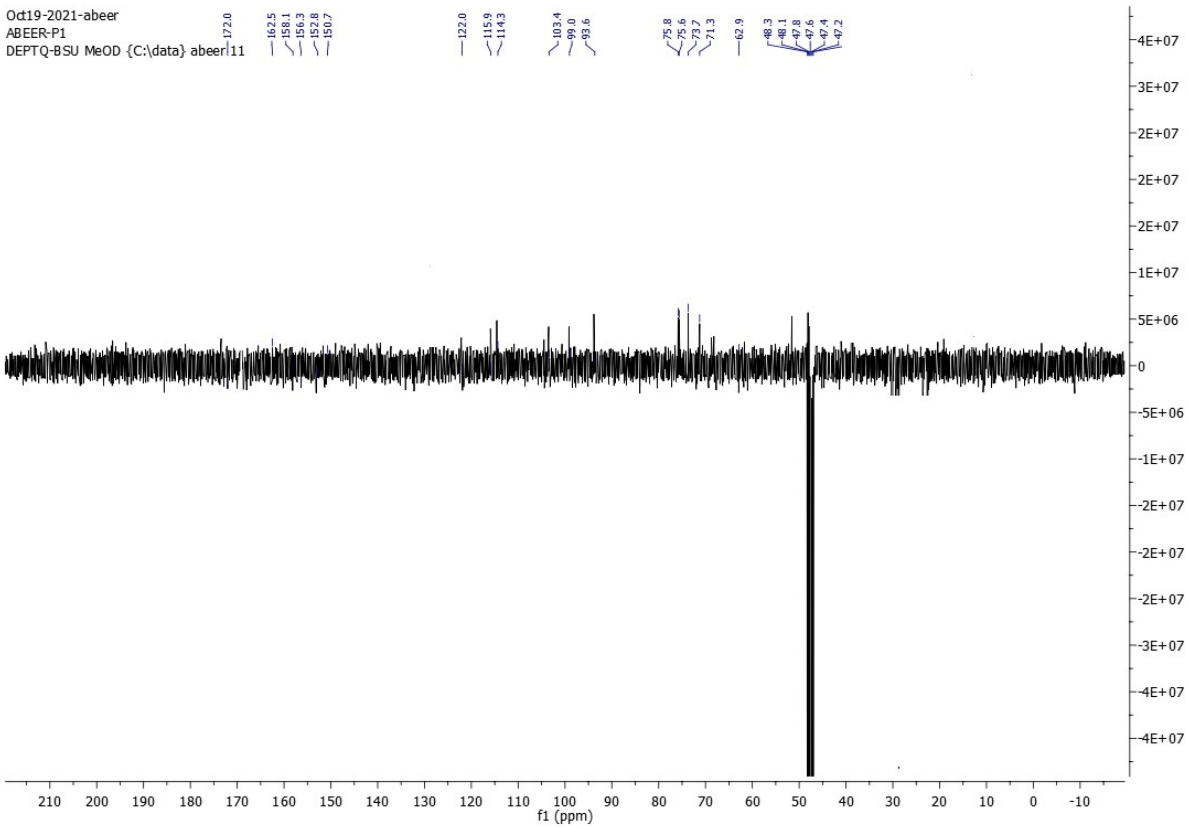

Figure S14. DEPT-Q NMR spectrum of compound **5** measured in CD_3OD-d_4 at 100 MHz

Figure S15. 1H NMR spectrum of compound **6** measured in CD_3OD-d_4 at 400 MHz

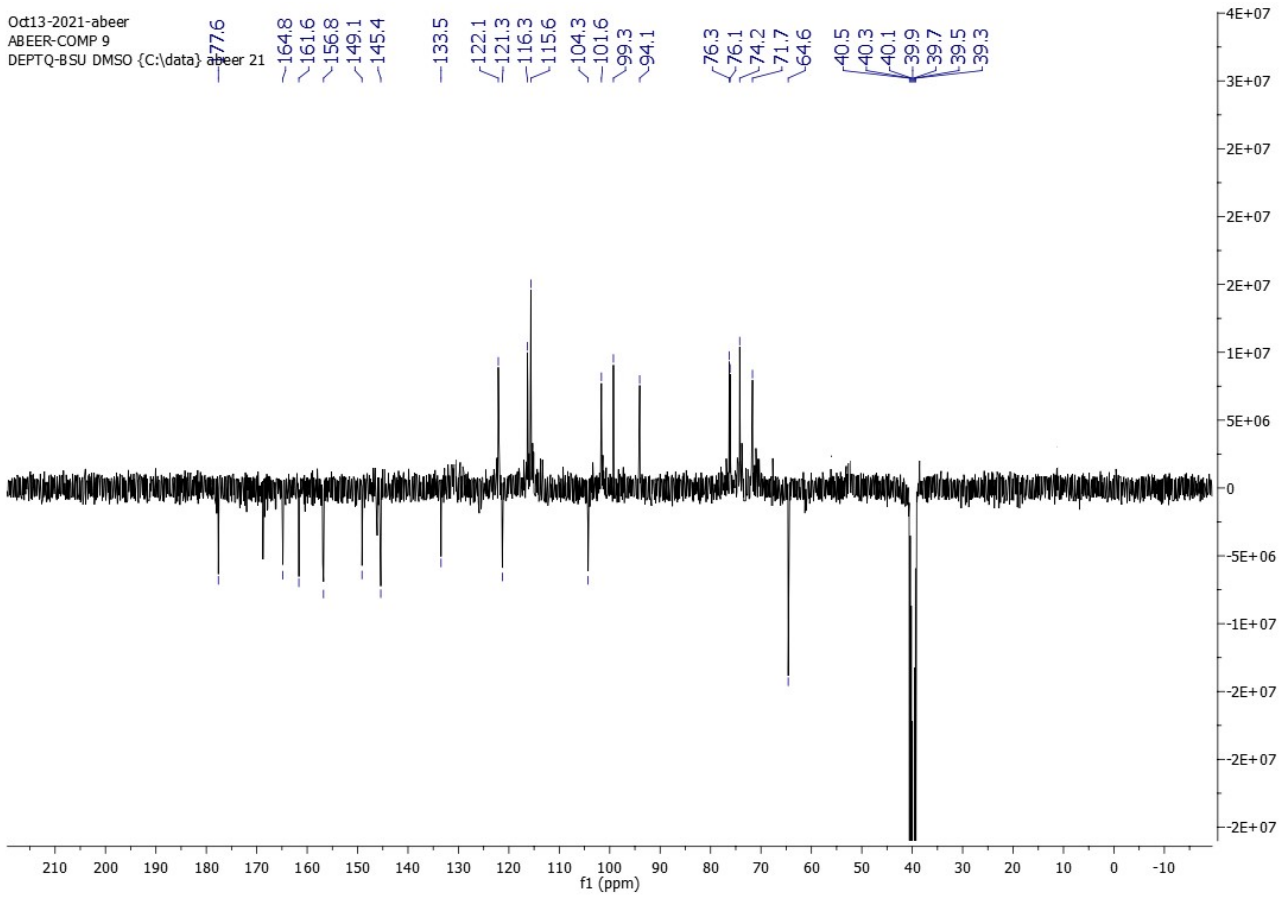

Figure S16. DEPT-Q NMR spectrum of compound **6** measured in CD_3OD-d_4 at 100 MHz

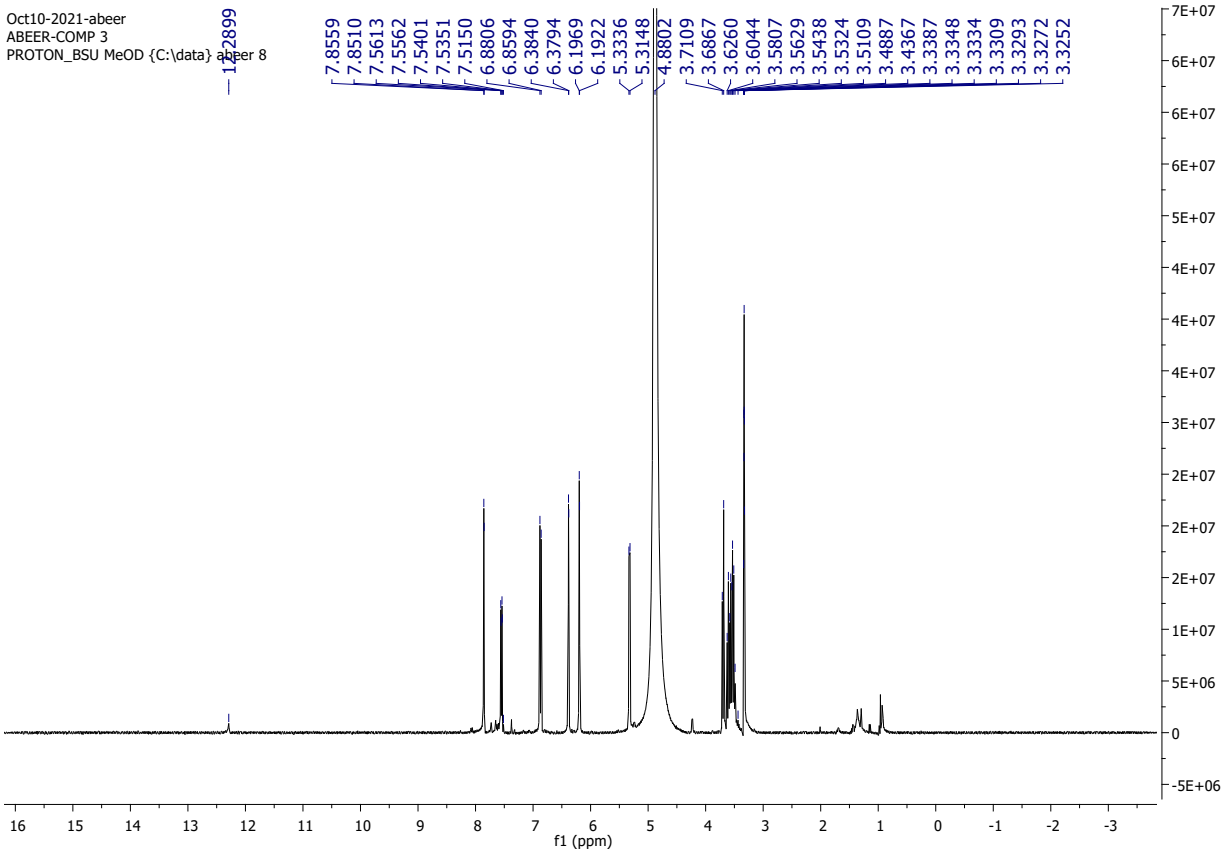

Figure S17. 1H NMR spectrum of compound **7** measured in CD_3OD-d_4 at 400 MHz

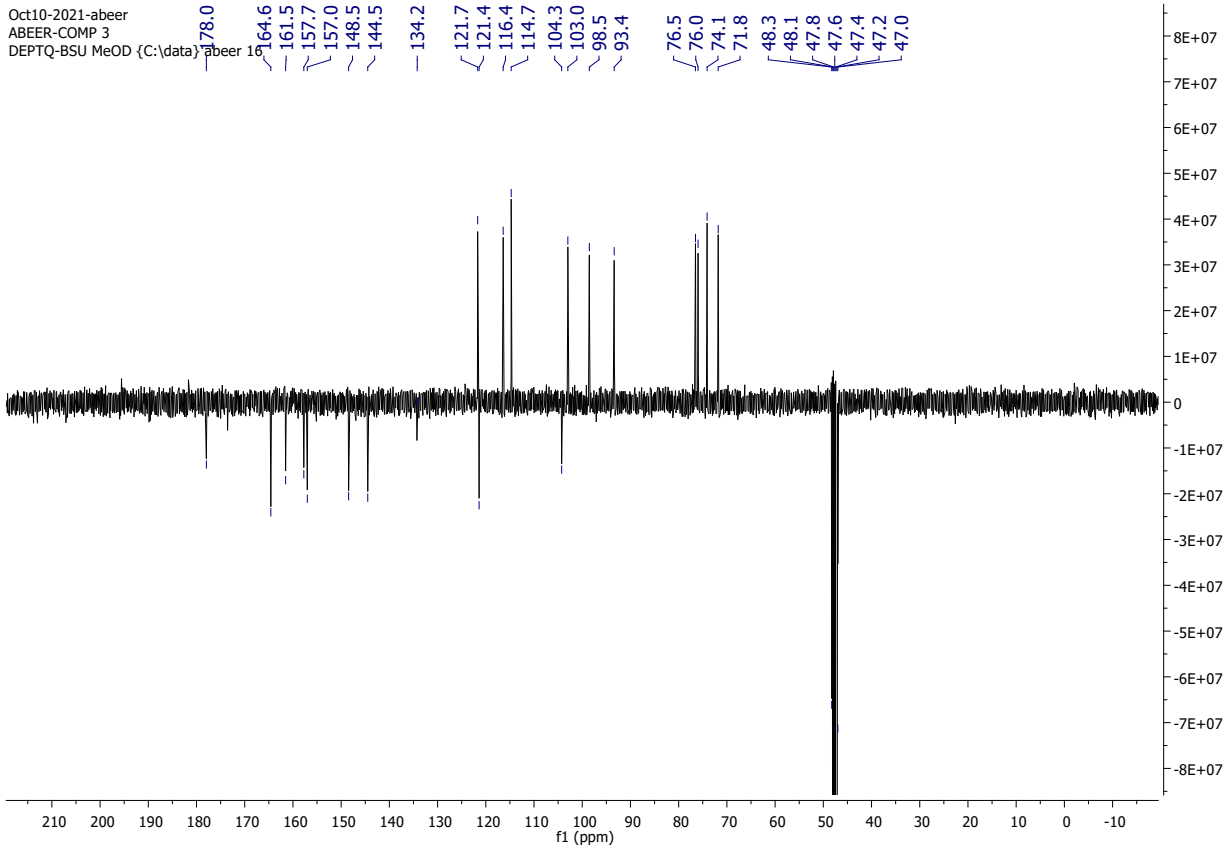

Figure S18. DEPT-Q NMR spectrum of compound **7** measured in CD_3OD-d_4 at 100 MHz

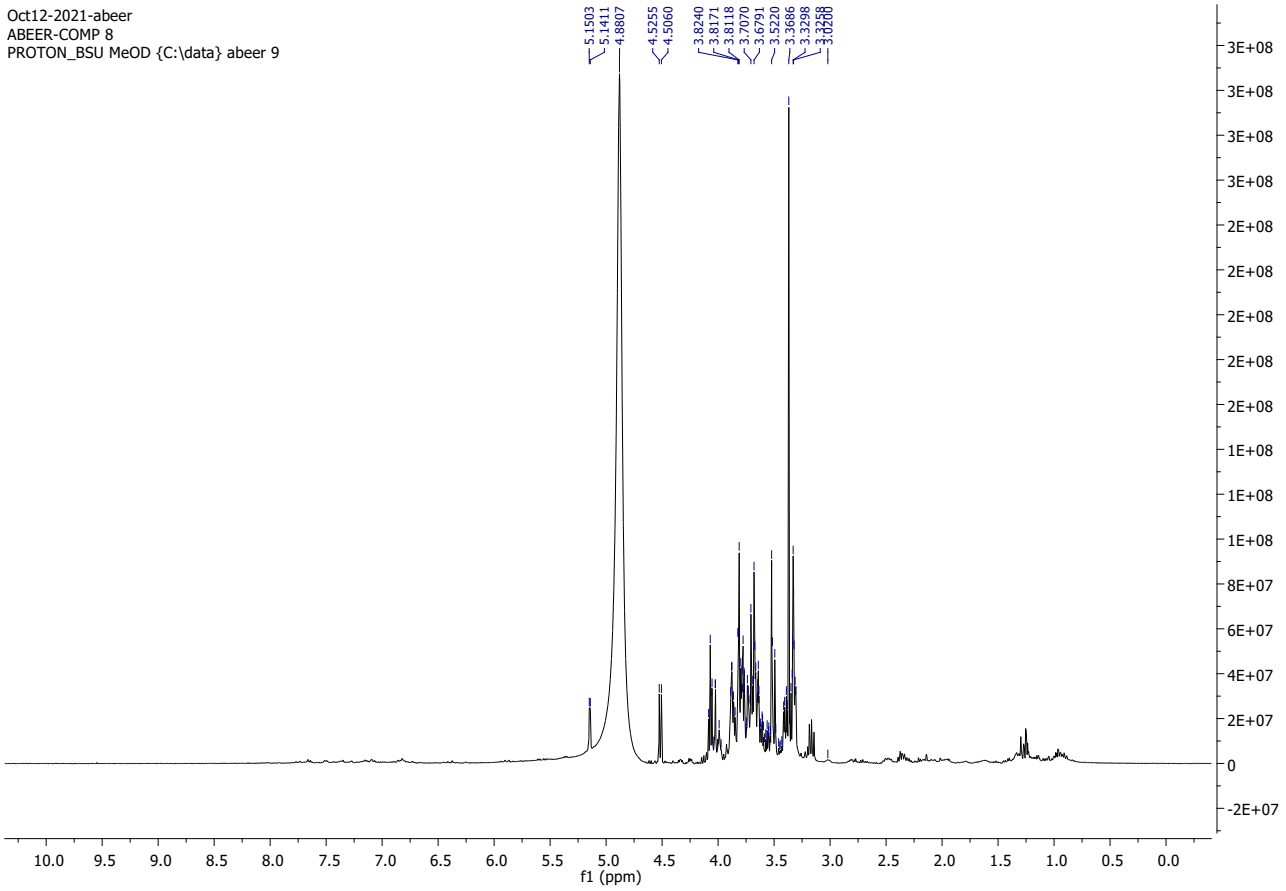

Figure S19. 1H NMR spectrum of compound **8** measured in CD_3OD-d_4 at 400 MHz

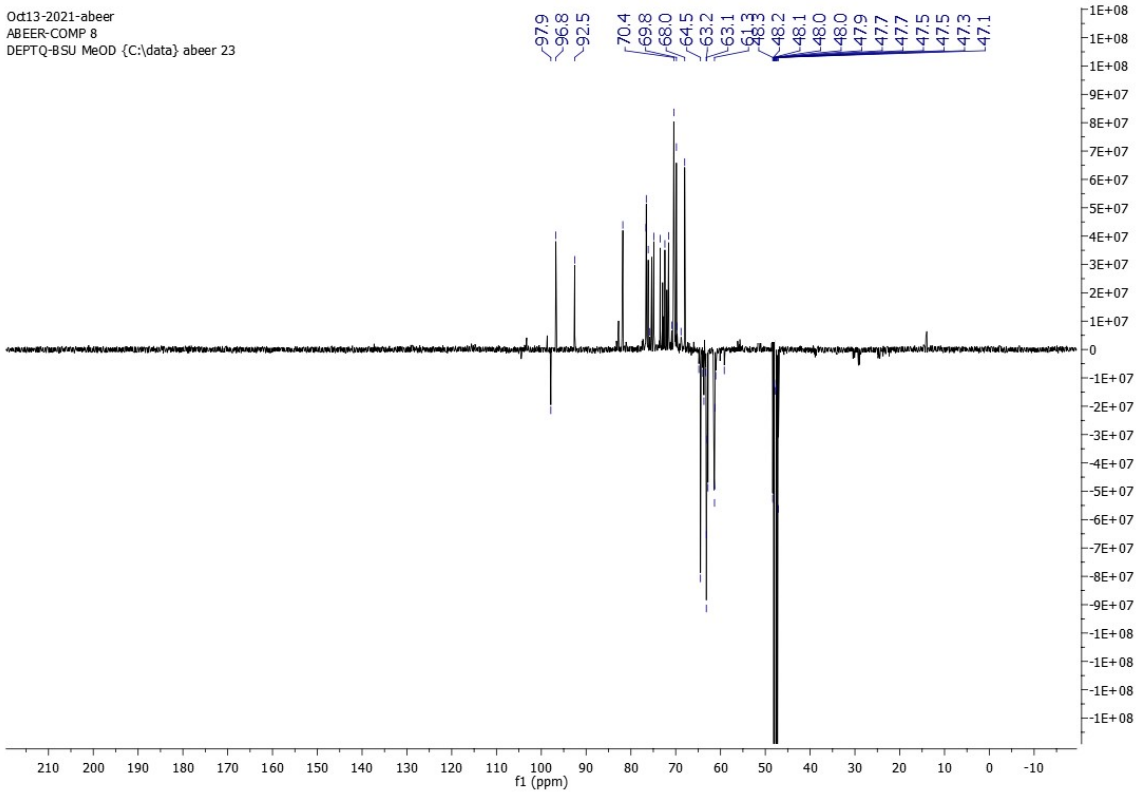

Figure S20. DEPT-Q NMR spectrum of compound **8** measured in CD_3OD-d_4 at 100 MHz

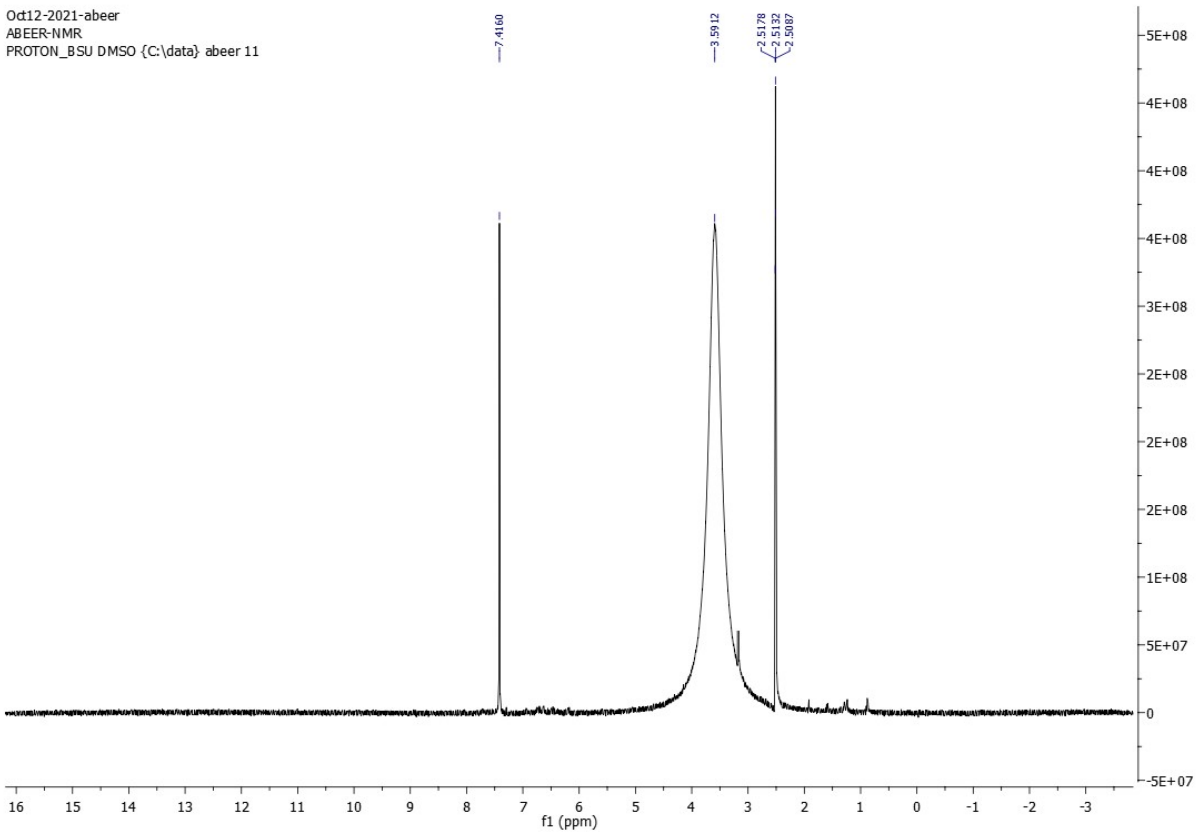

Figure S21. 1H NMR spectrum of compound **9** measured in DMSO-d_6 at 400 MHz

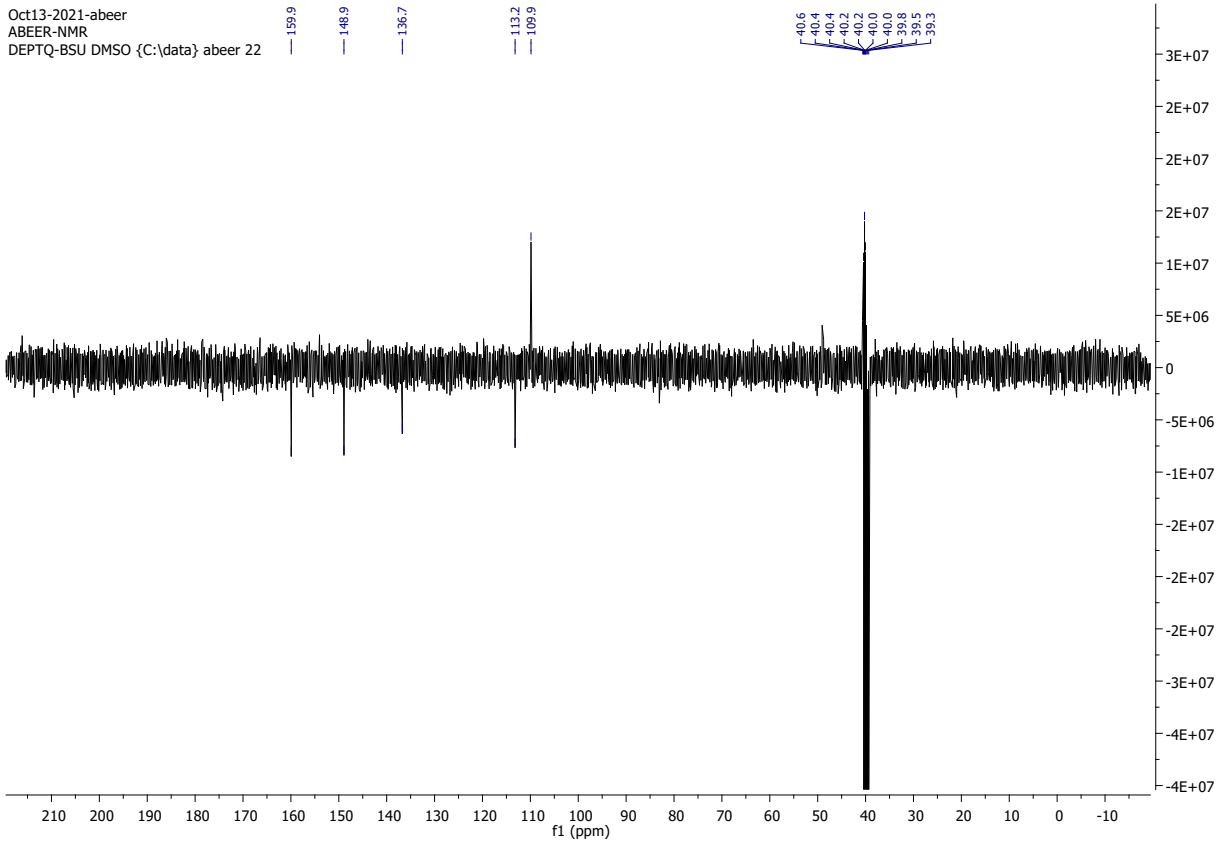

Figure S22. DEPT-Q NMR spectrum of compound **9** measured in DMSO-d_6 at 100 MHz

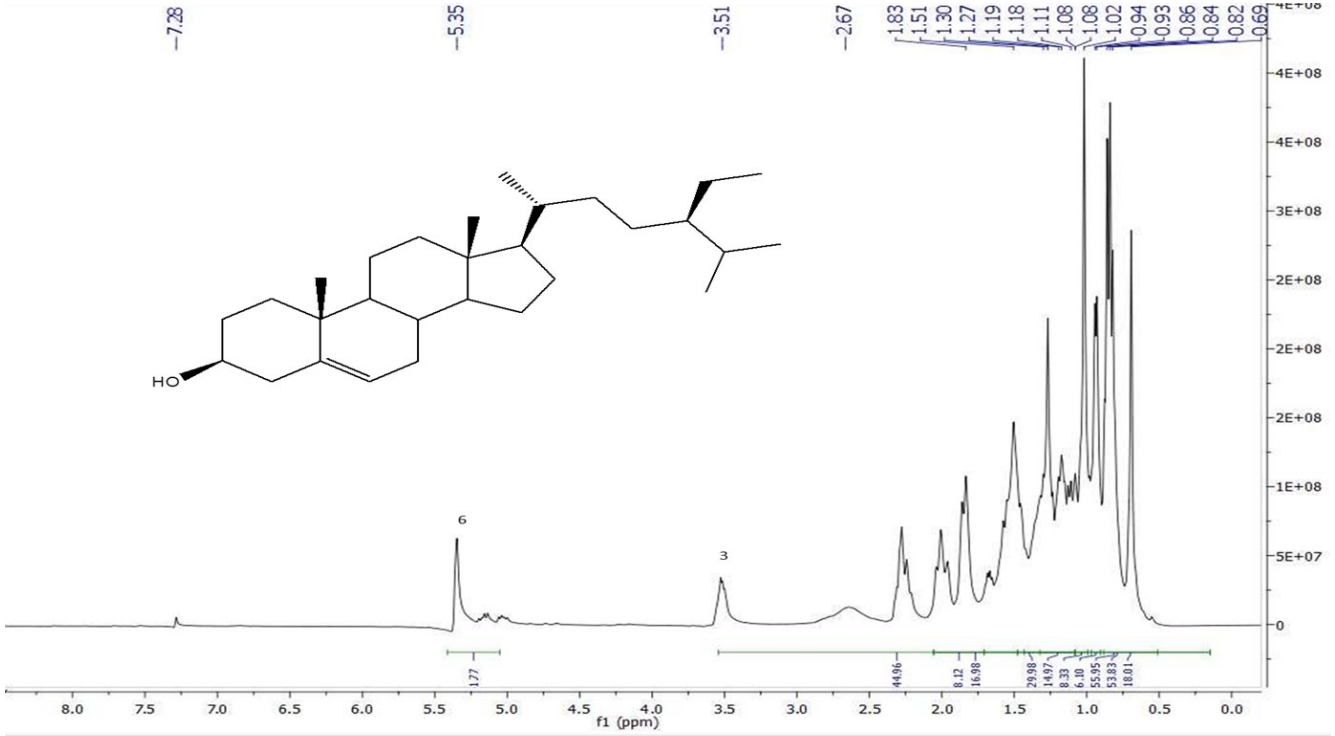

Figure S23. ^{1}H NMR spectrum of compound **10** measured in $CDCL_3$-*d* at 400 MHz

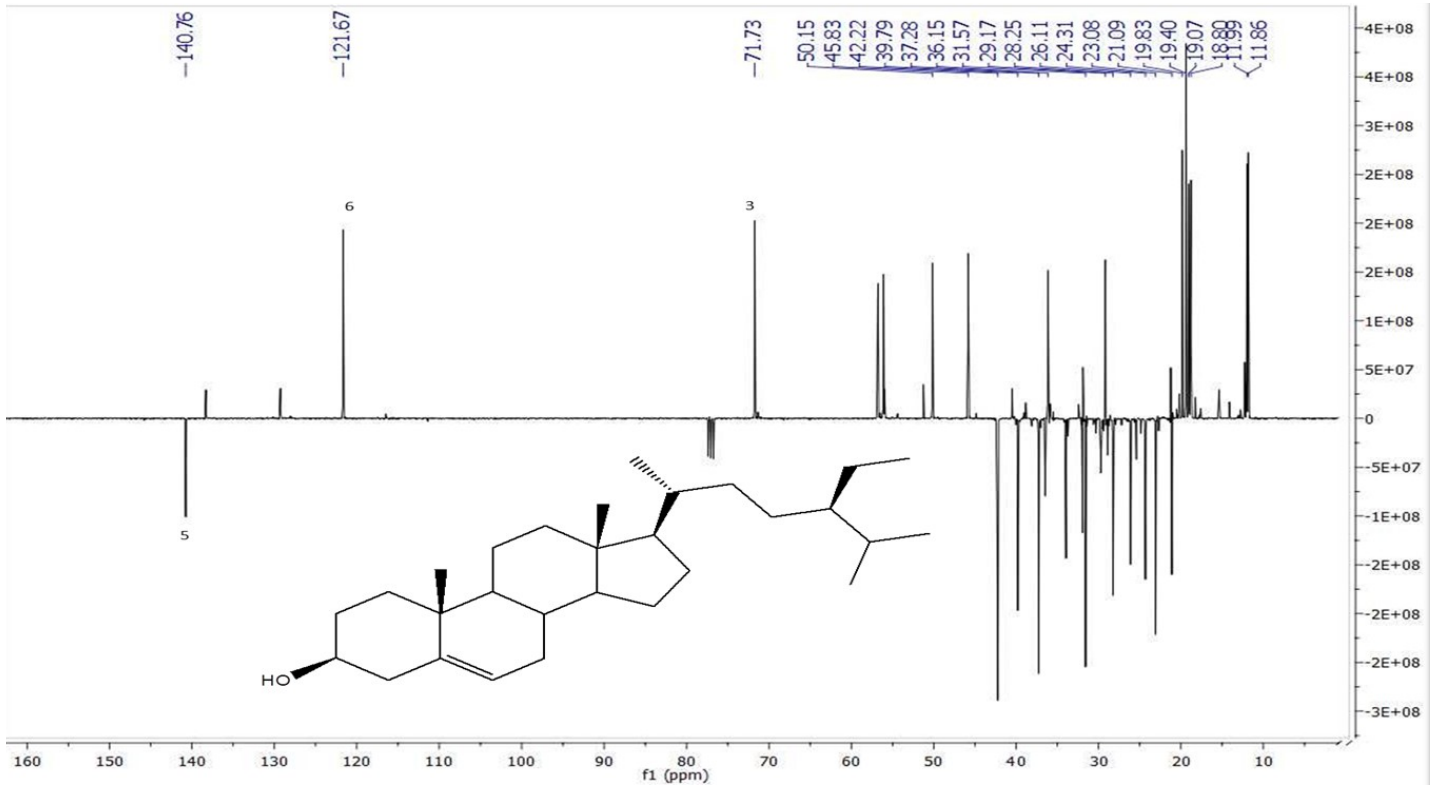

Figure S24. DEPT-Q NMR spectrum of compound **10** measured in $CDCL_3$-*d* at 100 MHz

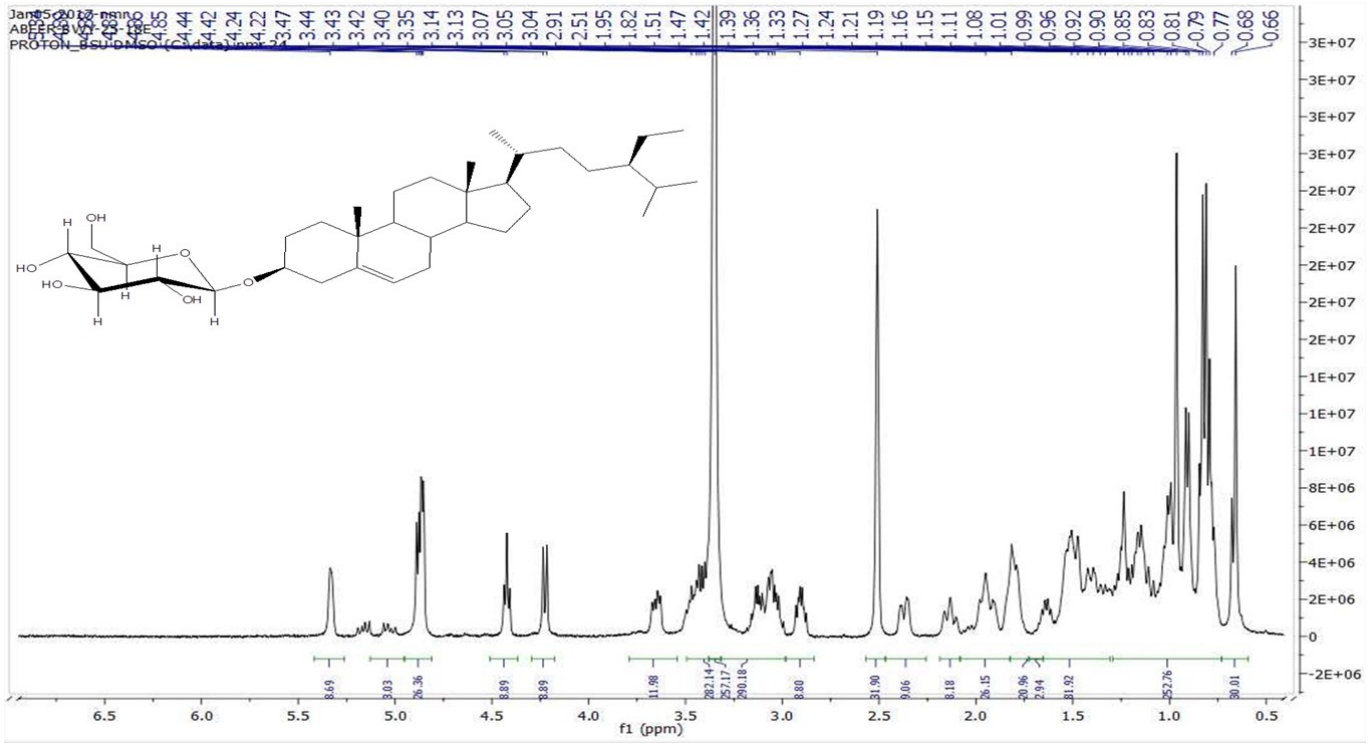

Figure S25. ^{1}H NMR spectrum of compound **11** measured in DMSO-d_6 at 400 MHz

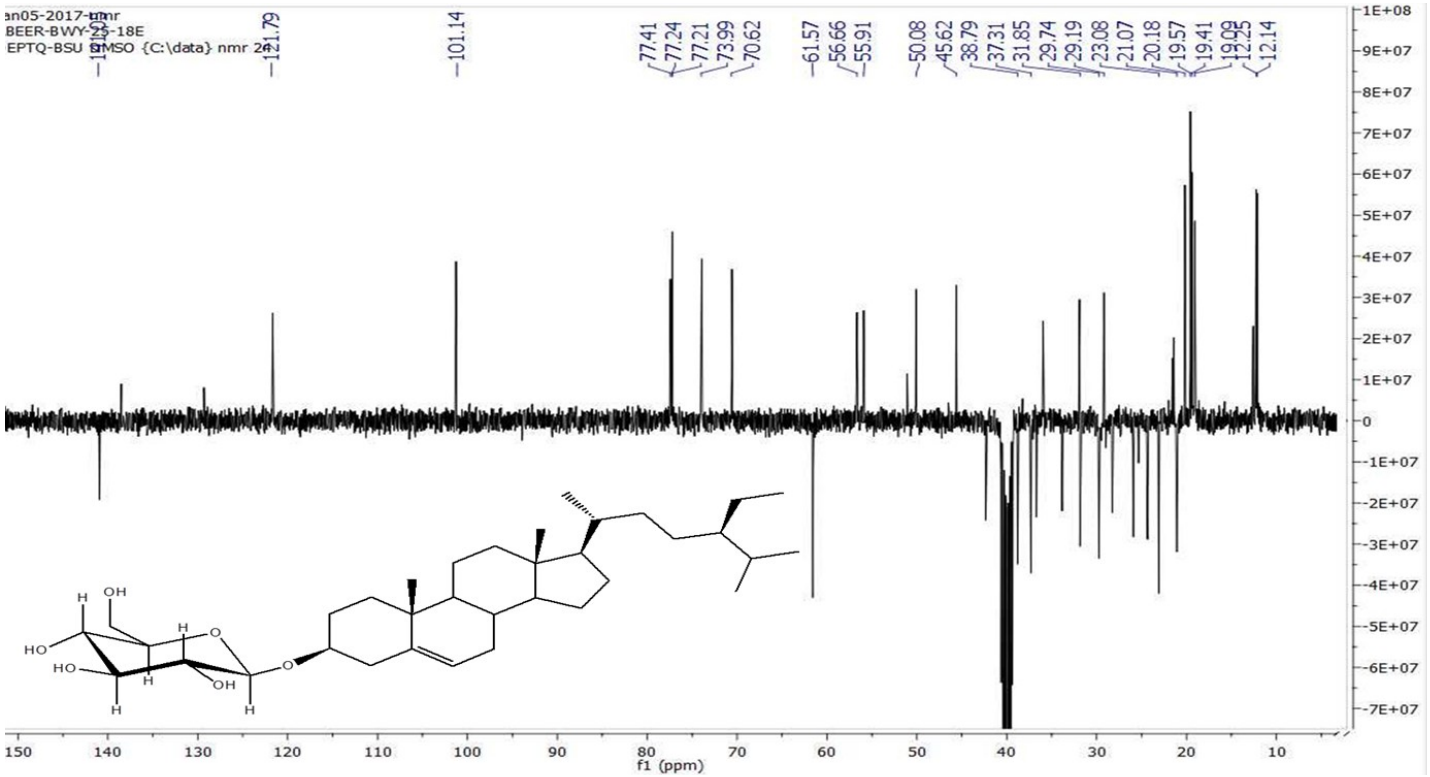

Figure S26. DEPT-Q NMR spectrum of compound **11** measured in DMSO-d_6 at 100 MHz

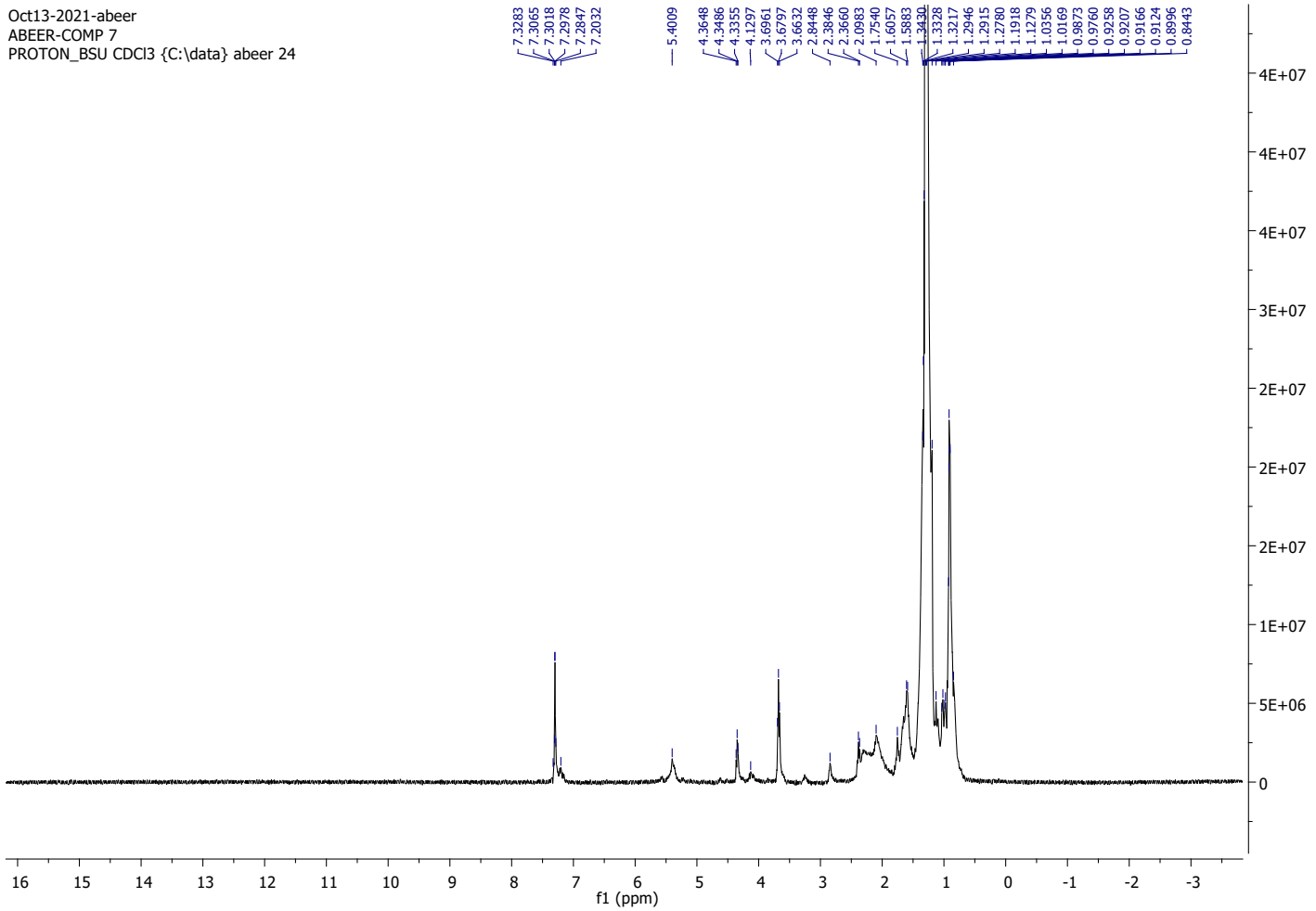

Figure S27. 1H NMR spectrum of compound **12** measured in $CDCL_3$-*d* at 400 MHz

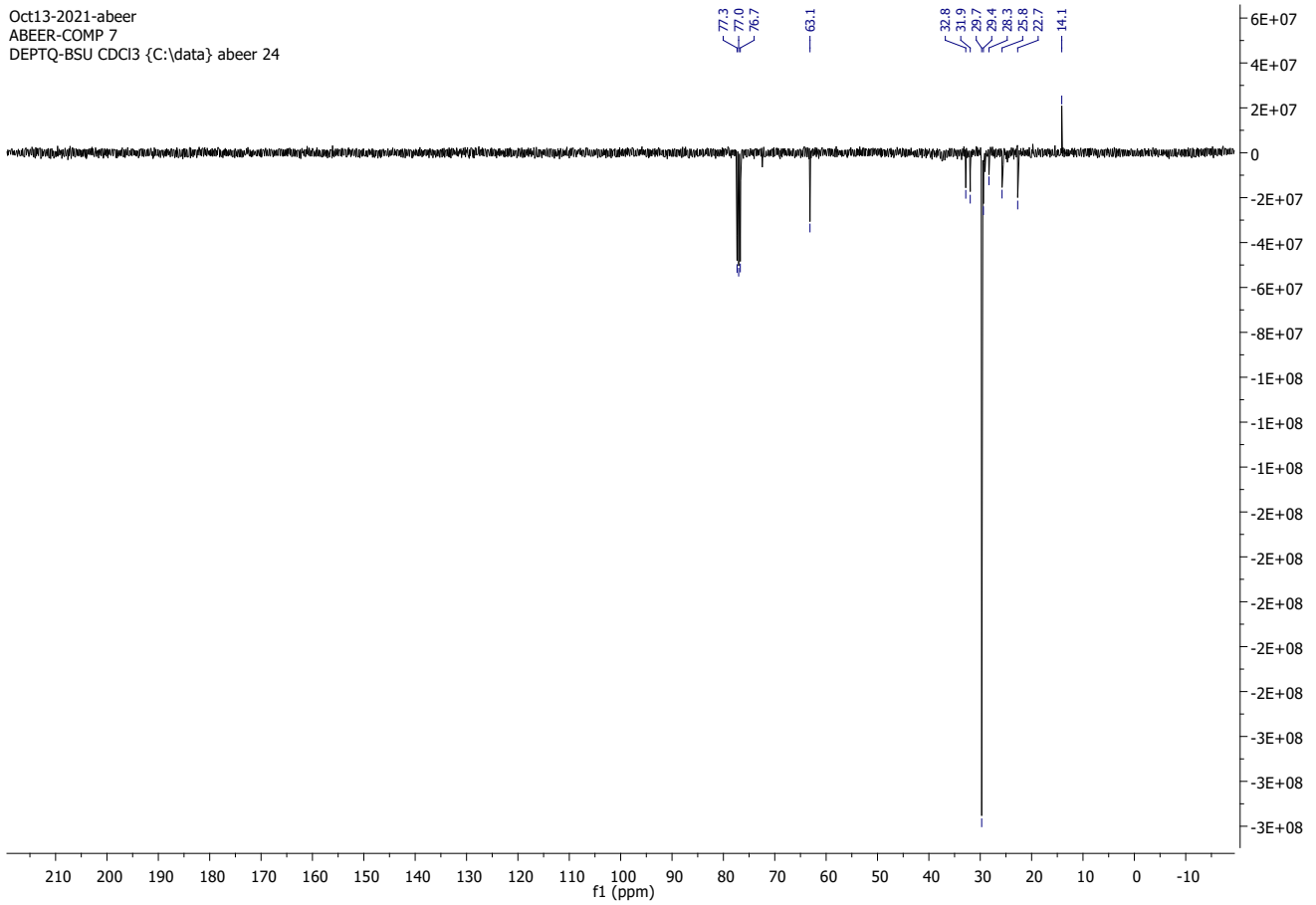

Figure S28. DEPT-Q NMR spectrum of compound **12** measured in $CDCL_3$-*d* at 100 MHz

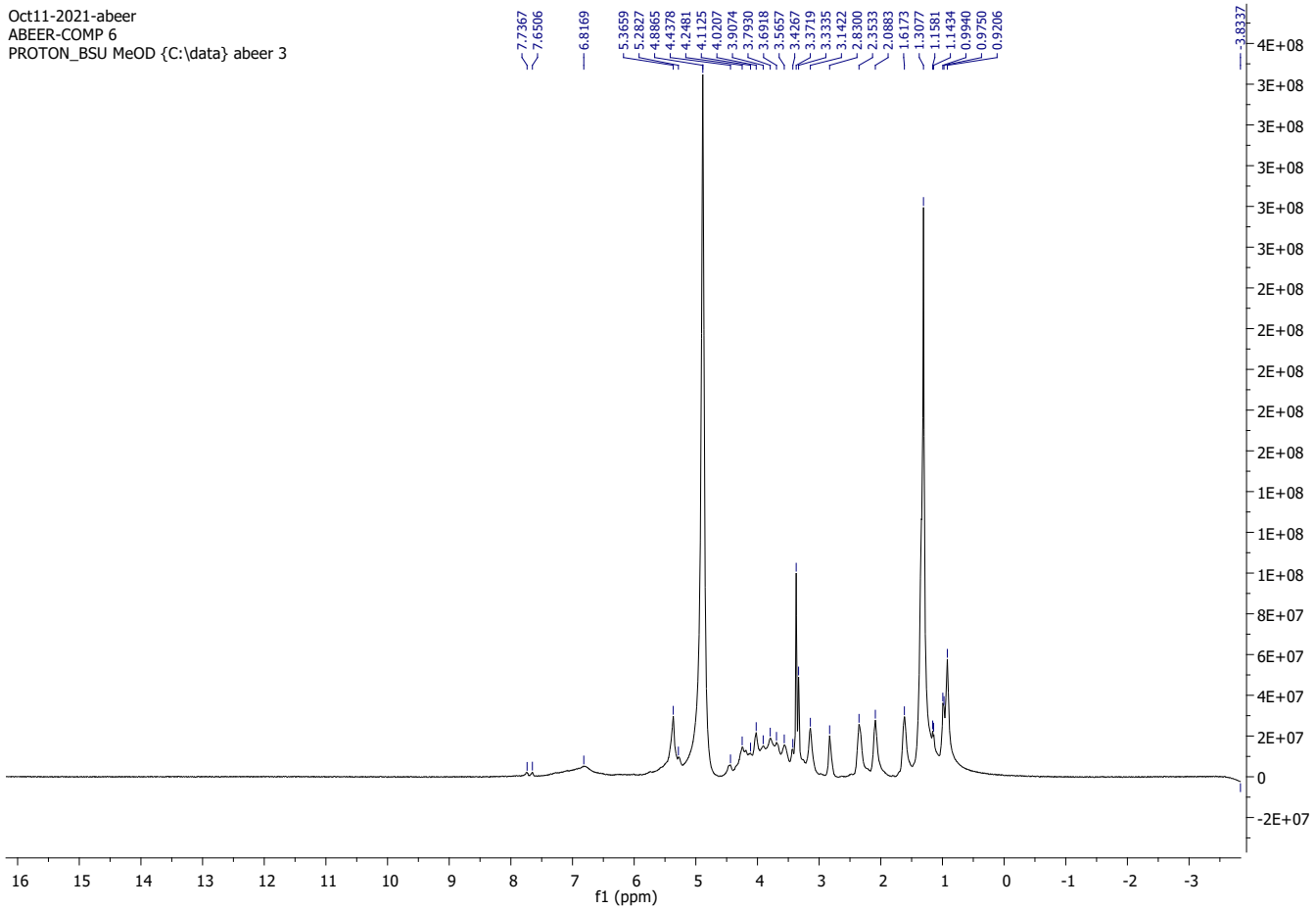

Figure S29. 1H NMR spectrum of compound **13** measured in CD_3OD-d_4 at 400 MHz

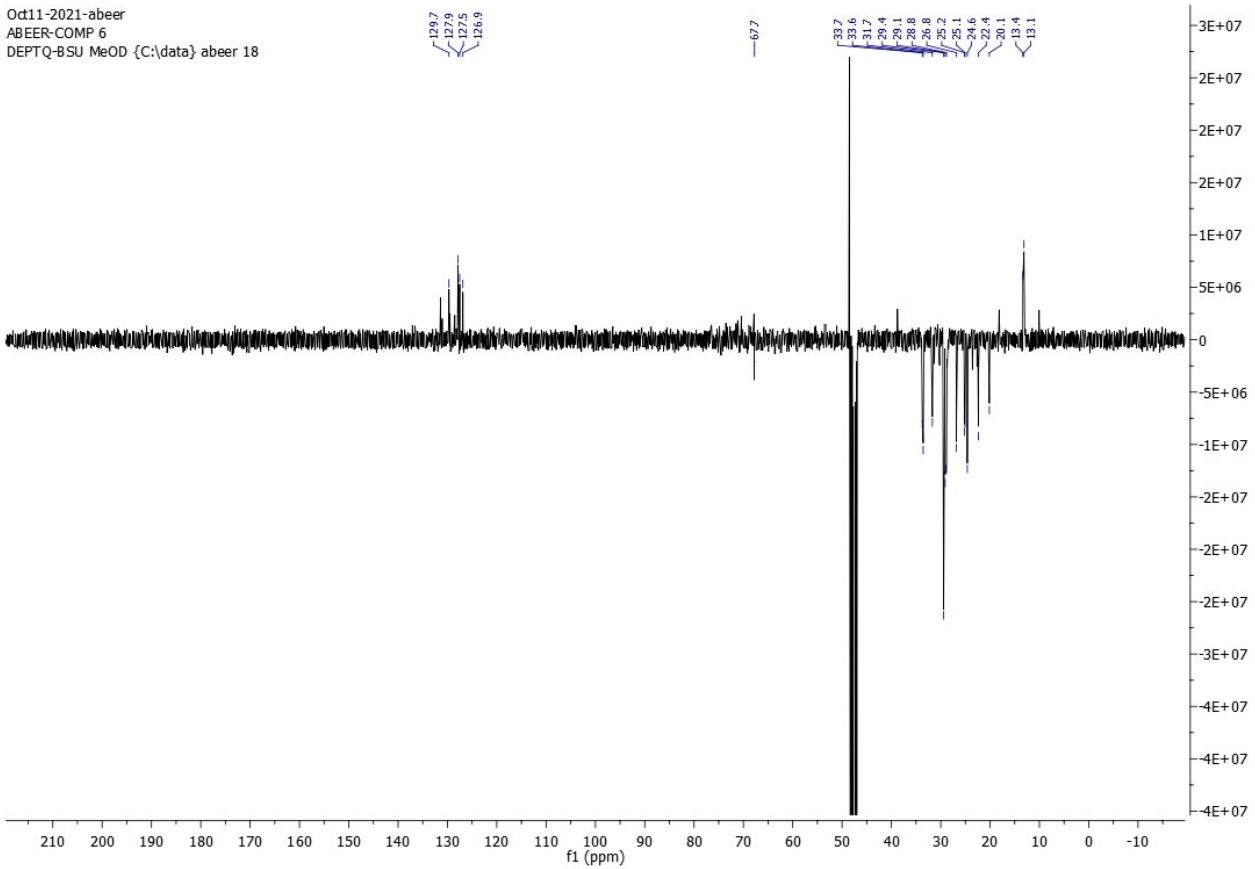

Figure S30. DEPT-Q NMR spectrum of compound **13** measured in CD_3OD-d_4 at 100 MHz

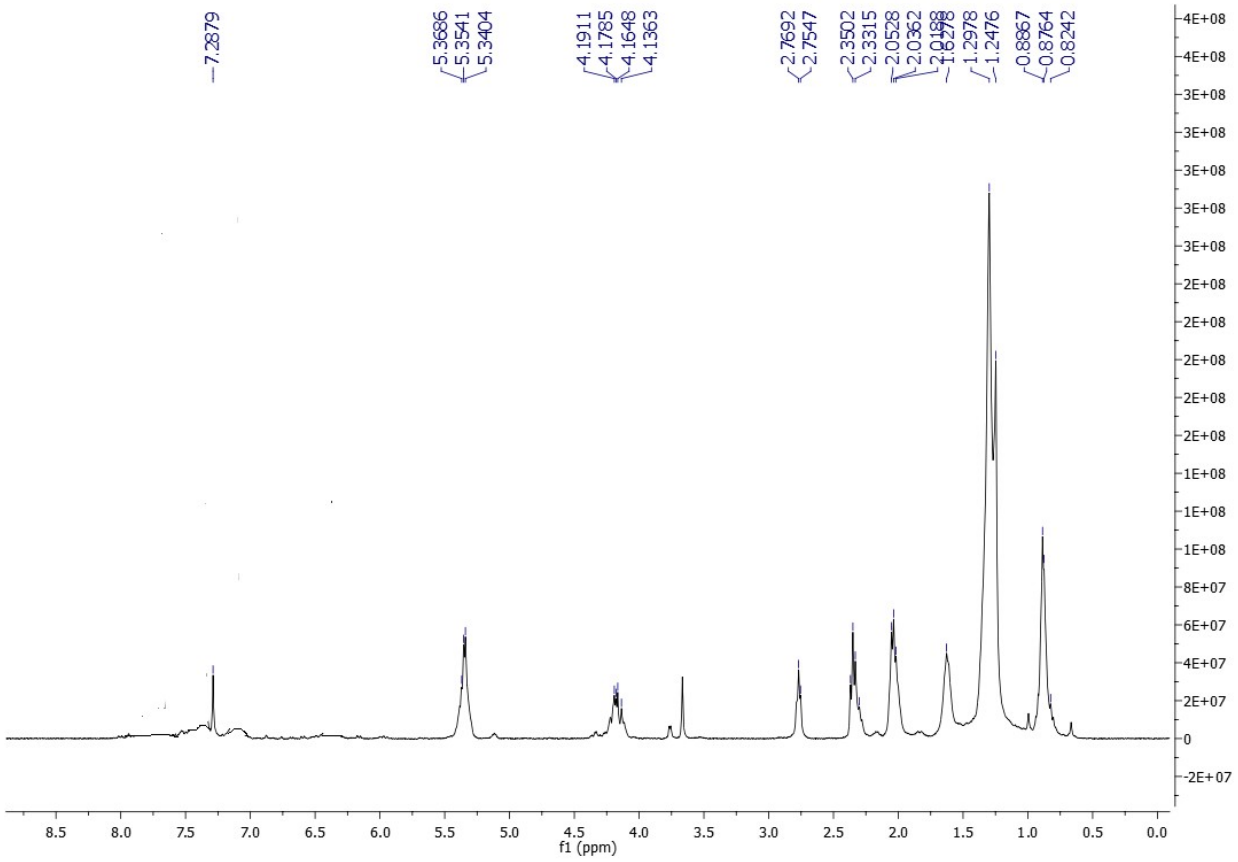

Figure S31.[1]H NMR spectrum of compound **14** measured in $CDCL_3$-*d* at 400 MHz

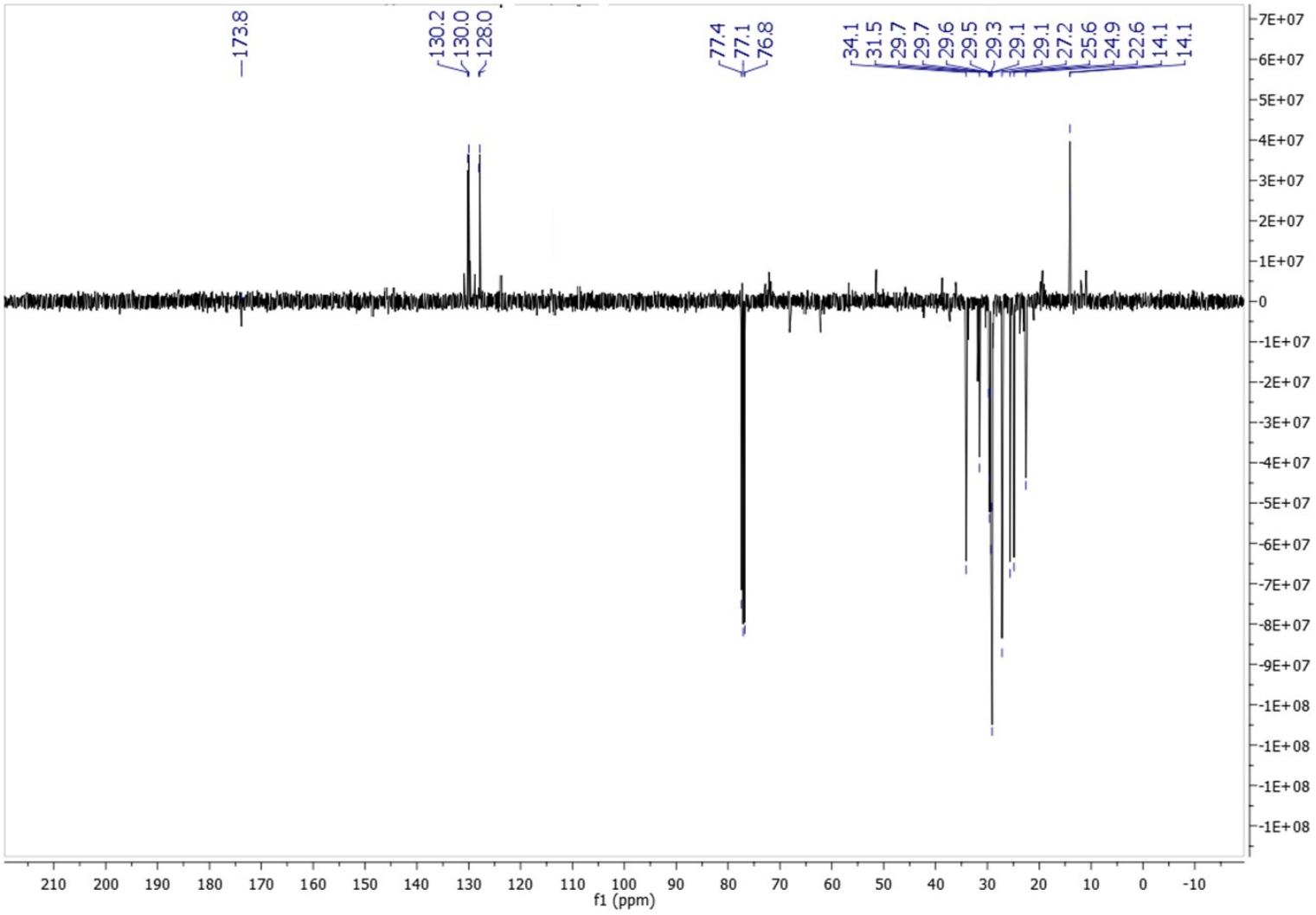

Figure S32. DEPT-Q NMR spectrum of compound **14** measured in $CDCL_3$-*d* at 100 MHz

Methods

Biological activity predictions using (PASS) software

The neural network-based software Prediction of Activity Spectra for Substances (PASS) [1] (www.way2drug.com) was used for further prioritization of the antimalarial activity of the suggested compounds (1–6). This software can predict > 4000 types of pharmacological and toxicological activities including their mechanism of action, with approximately 85% as acceptable precision, depending on the submitted compound structures that were subsequently screened utilizing the structure–activity relationship database (SARBase). The prediction results were expressed as probability scores (probably active "Pa" or probably inactive "Pi"). These calculated probability scores were determined by linking the structure and functional groups features in the tested molecules that matched or mismatched the specific activities listed in the software-associated database. The higher the Pa values, the more probable the compound to display the suggested pharmacological activity on a scale of 0–1. Pa values higher than 0.5 mean high experimental chance of the suggested pharmacological activity.

Molecular Docking

AutoDock Vina software was used in all molecular docking experiments [2]. All isolated compounds were docked against the Mpro crystal structure (PDB codes: 4PD4) [3]. The binding site was determined according to the enzyme's co-crystallized ligand. The co-ordinates of the grid box were: x = 76.11; y = -44.04; z = 23.45. The size of the grid box was set to be 10 Å. Exhaustiveness was set to be 24. Ten poses were generated for each docking experiment. Docking poses were analyzed and visualized using Pymol software [2].

References

1- Lagunin, A., Stepanchikova, A., Filimonov, D. & Poroikov, V. PASS: Prediction of activity spectra for biologically active substances. *Bioinformat.* **16**, 747–748 (2000).

2- Seeliger, D.; de Groot, B.L. Ligand docking and binding site analysis with PyMOL and Autodock/Vina. J. Comput. Aided Mol. Des. 2010, 24, 417–422.

3- Zhang, J., Yang, Q., Romero, J. A. C., Cross, J., Wang, B., Poutsiaka, K. M., ... & Dolle, R. E. (2015). Discovery of indazole derivatives as a novel class of bacterial gyrase B inhibitors. *ACS medicinal chemistry letters*, *6*(10), 1080-1085.